The mTORC1-mediated activation of ATF4 promotes protein and glutathione synthesis downstream of growth signals

Margaret E. Torrence[1], Michael R. MacArthur[1,4], Aaron M. Hosios[1], Alexander J. Valvezan[2], John M. Asara[3], James R. Mitchell[1,4], Brendan D. Manning[1, †]

[1]Department of Molecular Metabolism, Harvard T. H. Chan School of Public Health, Boston, MA 02115, USA

[2]Center for Advanced Biotechnology and Medicine, Department of Pharmacology, Rutgers Robert Wood Johnson Medical School, Piscataway, NJ 08854, USA

[3]Division of Signal Transduction, Beth Israel Deaconess Medical Center and Department of Medicine, Harvard Medical School, Boston, MA 02115, USA

[4]Department of Health Sciences and Technology, Swiss Federal Institute of Technology (ETH) Zurich, 8603 Zurich, Switzerland

[†]Corresponding author. E-mail: bmanning@hsph.harvard.edu

Abstract

The mechanistic target of rapamycin complex 1 (mTORC1) stimulates a coordinated anabolic program in response to growth-promoting signals. Paradoxically, recent studies indicate that mTORC1 can activate the adaptive stress-responsive transcription factor ATF4 through mechanisms distinct from its canonical induction by the integrated stress response (ISR). However, how ATF4 functions in response to these distinct modes of regulation and its broader role as a downstream target of mTORC1 are unknown. Therefore, we directly compared ATF4-dependent transcriptional changes induced upon activation of mTORC1 or the ISR. The mTORC1-ATF4 pathway stimulated the expression of only a subset of the ATF4 target genes stimulated by the ISR, including genes involved in amino acid uptake, synthesis, and tRNA charging. We demonstrate that ATF4 is a metabolic effector of mTORC1 involved in both its established role in promoting protein synthesis and in a previously unappreciated function for mTORC1 in stimulating cellular cystine uptake and glutathione synthesis.

Introduction

Pro-growth signals in the form of growth factors, hormones, and nutrients impinge on cellular metabolic programs in a coordinated fashion involving both acute, post-translational regulation and transcriptional control of nutrient transporters and metabolic enzymes. The mechanistic target of rapamycin complex 1 (mTORC1) acts as a central point of integration for these signals and propagates a downstream metabolic response that increases anabolic processes while decreasing specific catabolic processes. Through a variety of downstream effectors, mTORC1 stimulates the synthesis of the major macromolecules comprising cellular biomass, including protein, lipid, and nucleic acids, along with metabolic and adaptive pathways that support this anabolic program (Valvezan & Manning, 2019).

A particularly interesting feature of this coordinated metabolic program downstream of mTORC1 is the co-opting of key nutrient-sensing transcription factors that are established to be activated, independent of mTORC1, in response to depletion of specific nutrients (Torrence & Manning, 2018). In their canonical roles, these transcription factors serve to mount an adaptive response by upregulating genes that allow cells to overcome the specific nutrient deficiency. Perhaps the best characterized of these transcription factors with dual regulation is the hypoxia-inducible factor 1 (HIF1) comprising the labile HIF1α protein heterodimerized with the aryl hydrocarbon receptor nuclear translocator (ARNT or HIF1β). Oxygen depletion (i.e., hypoxia) results in the rapid stabilization of HIF1α and allows the HIF1 heterodimer to induce genes involved in glucose uptake, glycolysis, and angiogenesis to adapt to hypoxia and decrease mitochondrial respiration (Nakazawa et al., 2016). On the other hand, in response to upstream growth factor signaling pathways, activation of mTORC1 stimulates an increase in HIF1α protein synthesis leading to elevated expression of HIF1 gene targets (J. B. Brugarolas et al., 2003; Duvel et al., 2010; Hudson et al., 2002; Laughner et al., 2001; Thomas et al., 2006; Zhong et al., 2000). The result is an mTORC1-mediated increase in glucose uptake and glycolysis even when oxygen is not limiting (e.g. normoxia), a process referred to as aerobic glycolysis, which can support the production of biosynthetic precursors in the form of glycolytic

59 intermediates. Similarly, the sterol regulatory element (SRE)-binding protein (SREBP)
60 family of transcription factors are independently regulated by both adaptive nutrient
61 signals and growth signals controlling mTORC1. The SREBPs are canonically activated
62 upon sterol depletion and induce expression of the enzymes required for de novo
63 synthesis of fatty acid and sterol lipids (Horton et al., 2002). However, insulin and growth
64 factor signaling can also induce lipid synthesis via mTORC1-stimulated activation of
65 SREBP and its lipogenic gene targets (Duvel et al., 2010; Owen et al., 2012; Peterson et
66 al., 2011; Porstmann et al., 2008). Recent studies have suggested that the regulation of
67 nutrient-sensing transcription factors by mTORC1 signaling extends to the activating
68 transcription factor 4 (ATF4) (Adams, 2007; Ben-Sahra et al., 2016; Torrence & Manning,
69 2018).
70
71 ATF4 is a basic leucine zipper (bZIP) transcription factor that is selectively translated in
72 response to specific forms of cellular stress to induce the expression of genes involved in
73 adaptation to stress (Walter & Ron, 2011). This adaptive program is referred to as the
74 integrated stress response (ISR) and is initiated by stress-activated protein kinases,
75 including general control nonderepressible 2 (GCN2) activated upon amino acid
76 deprivation and protein kinase RNA-like endoplasmic reticulum kinase (PERK) activated
77 by ER stress, among others, which phosphorylate eIF2α on Ser51 (Harding et al., 2000).
78 Phosphorylation of eIF2α serves to globally attenuate mRNA translation to conserve
79 amino acids and energy and decrease the cellular protein load as one adaptive measure
80 to overcome these stresses (Clemens, 1996). Importantly, a small number of mRNAs,
81 including that encoding ATF4, exhibit increased translation upon eIF2α-Ser51
82 phosphorylation (Vattem & Wek, 2004). The stress-induced increase in ATF4 leads to the
83 expression of a canonical set of ATF4 target genes, including those involved in non-
84 essential amino acid biosynthesis and amino acid transport, as part of the adaptive
85 cellular response specific to stresses such as amino acid depletion (Harding et al., 2003).
86 ATF4 functions in heterodimers with other bZIP transcription factors and also co-regulates
87 many of its target genes with additional transcription factors as part of the cellular stress
88 response (Newman & Keating, 2003; Wortel et al., 2017). However, whether and how the

many distinct upstream stresses that activate ATF4 influence its heterodimerization partners and the induction of specific sets of genes is not well understood.

While ATF4 is a major downstream effector of the ISR, evidence has emerged that ATF4 can also be activated by pro-growth signals that stimulate mTORC1 signaling (Adams, 2007; Ben-Sahra et al., 2016), and cis-regulatory elements for ATF4 binding are enriched in the promoters of mTORC1-induced genes (Duvel et al., 2010). Importantly, the mTORC1-mediated activation of ATF4 involves its increased translation in a manner that is independent of the ISR and phosphorylation of eIF2α (Ben-Sahra et al., 2016; Park et al., 2017). These findings suggest that, similar to HIF1 and SREBP, ATF4 induction may be mobilized as part of the broader anabolic program downstream of mTORC1. Indeed, our previous findings indicate that mTORC1 promotes *de novo* purine synthesis, in part, through induction of mitochondrial one-carbon metabolism via ATF4 activation and expression of its gene target MTHFD2 (Ben-Sahra et al., 2016).

How the ATF4-dependent gene program compares between its adaptive role in the ISR and its activation as a downstream effector of mTORC1 signaling and whether ATF4 contributes to established or new functions of mTORC1 are unknown (Figure 1A). Here, we find that the mTORC1-ATF4 program represents a small subset of ATF4-dependent genes induced by ER stress and includes genes encoding the enzymes required for tRNA charging, non-essential amino acid synthesis, and amino acid uptake. Consistent with regulation of these enzymes by mTORC1 through ATF4, ATF4 contributes to the induction of protein synthesis downstream of mTORC1. We also find that mTORC1 signaling promotes glutathione synthesis through ATF4 and its specific regulation of the cystine transporter SLC7A11. Thus, ATF4 is an anabolic effector of mTORC1 signaling, necessary for both its canonical regulation of protein synthesis and its induced synthesis of glutathione, the most abundant anti-oxidant in cells.

Results

mTORC1 signaling activates a subset of ATF4-dependent genes also activated by the integrated stress response

To identify the ATF4-dependent gene targets downstream of mTORC1, we compared the insulin-induced, rapamycin-sensitive transcripts between wild-type MEFs and those with biallelic loss of ATF4 via CRISPR/Cas9 gene deletion (see methods). Consistent with our previous studies (Ben-Sahra et al., 2016), insulin stimulated an increase in ATF4 protein in MEFs, which was decreased with rapamycin (Figure 1B—quantified in figure supplement 1). In parallel, these cells were treated with a time course of tunicamycin, an inhibitor of N-glycosylation that potently induces ER stress and an increase in ATF4, to identify ATF4 gene targets downstream of the ISR. RNA-seq analysis revealed that 20% of transcripts (253 total) significantly upregulated upon insulin stimulation were significantly blocked in their induction with rapamycin treatment. Approximately 30% of these mTORC1-regulated genes (77 total) lost their insulin responsiveness with ATF4 deletion. In comparison, 36% of transcripts significantly induced with tunicamycin treatment at 4 hours were dependent on ATF4 (774 total). Importantly, the expression of just 61 genes was found to overlap between these two modes of ATF4 regulation, being ATF4 dependent in response to both mTORC1 activation and the ISR (Figure 1C—supplementary table 1).

The RNA-seq analysis demonstrated that only 8% of ATF4 gene targets induced by ER stress were also significantly stimulated by mTORC1 signaling (e.g., insulin induced and rapamycin sensitive). Interestingly, these 61 shared genes showed significant KEGG pathway enrichment for aminoacyl tRNA biosynthesis, amino acid metabolism, and one-carbon metabolism (Figure 1D). The genes shared between the ISR and mTORC1 signaling were greatly enriched amongst those exhibiting the most significant increase upon tunicamycin treatment, with 75% (46 genes) lying within the top 100 of the 774 tunicamycin-induced genes (Figure 1E). It is worth noting that many of the top ATF4-dependent genes that scored as being induced by the ISR alone showed some degree of rapamycin-sensitive induction with insulin but did not reach statistical significance in the RNA-seq analyses. These data indicate that the subset of ATF4-dependent genes induced by mTORC1 signaling are largely comprised of those that are also most sensitive

Figure 1

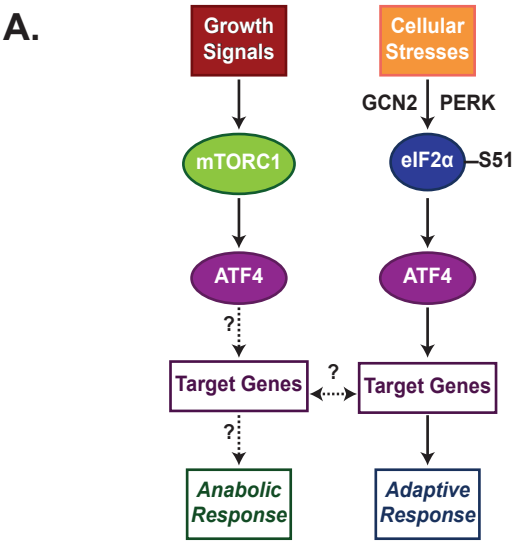

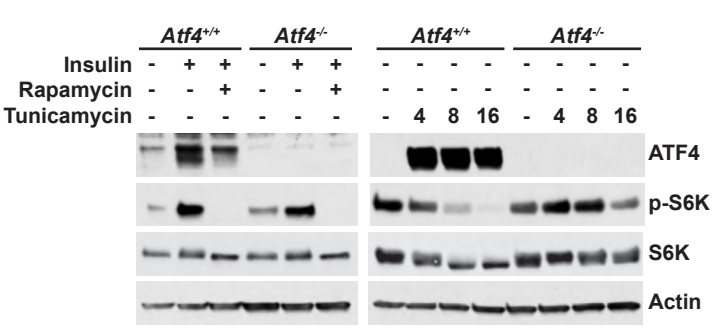

D.

Shared mTORC1 and ISR KEGG Enrichment

Function	P Value
Aminoacyl tRNA Biosynthesis	1.19E-07
Gly, Ser, and Thr Metabolism	7.85E-05
1-Carbon Metabolism	7.85E-05
Cys and Met Metabolism	.0001894
Ala, Asp, and Gln Metabolism	.01337497

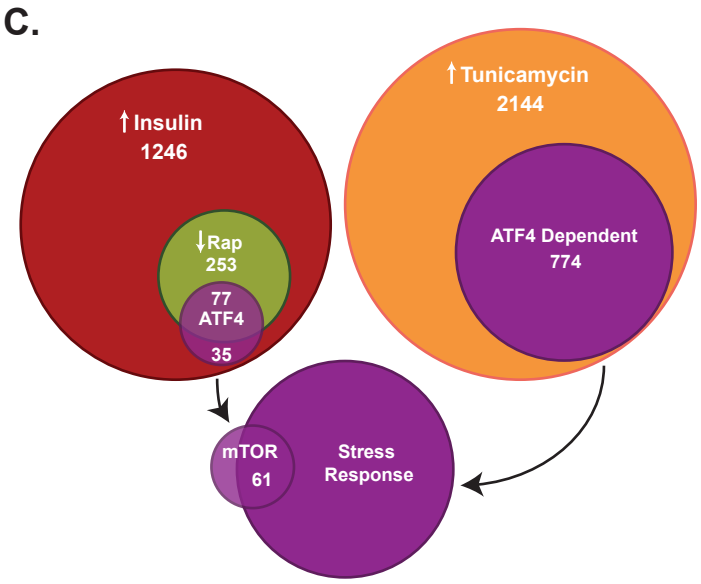

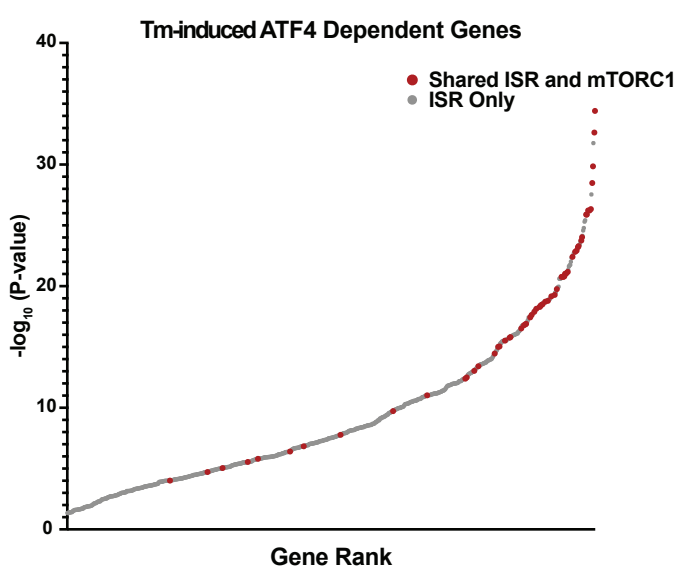

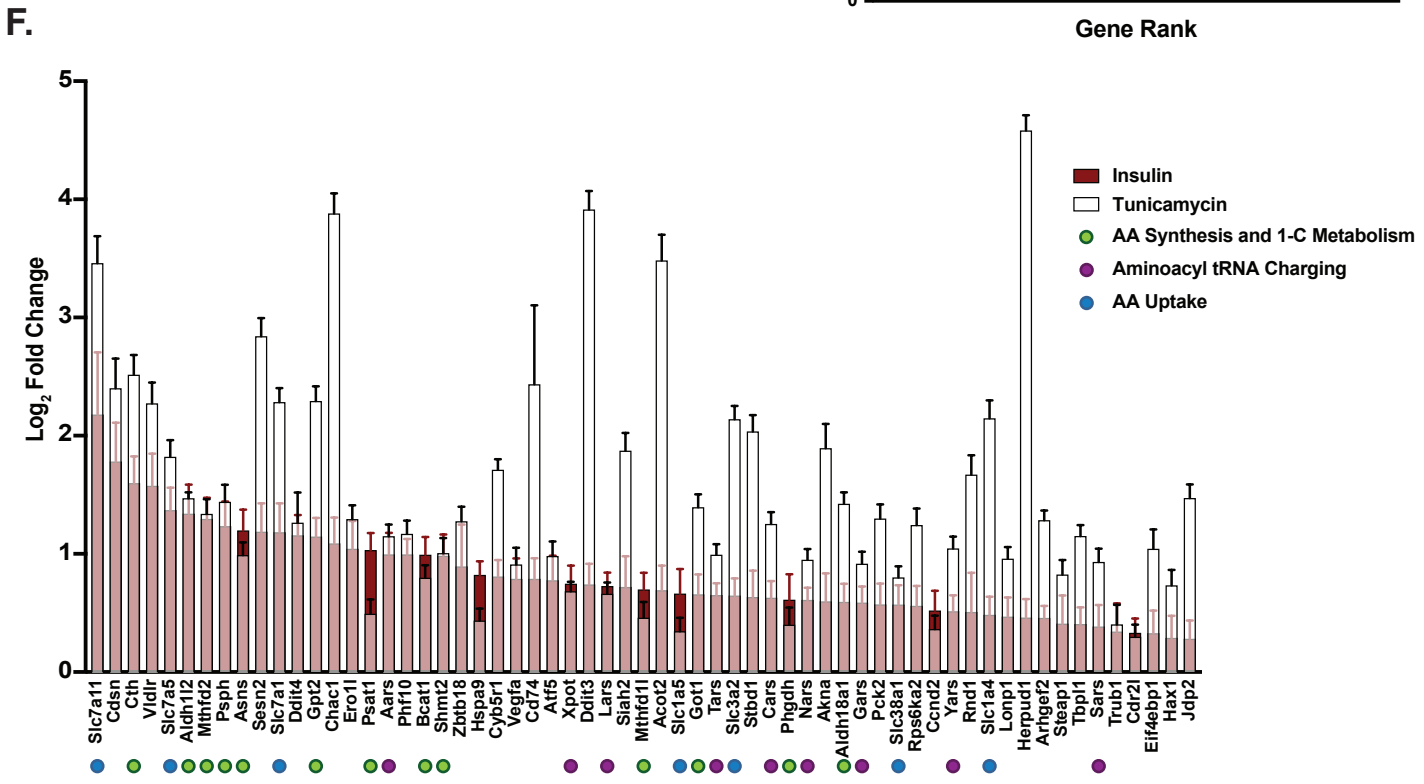

Figure 1. mTORC1 signaling activates a subset of ATF4-dependent genes also activated by the integrated stress response.

(A) Schematic of the dual regulation of ATF4 and the unknowns addressed in this study.

(B) Immunoblots of parallel lysates from RNA-Seq experiment. *Atf4*$^{+/+}$ and *Atf4*$^{-/-}$ MEFs were treated, as indicated, with insulin (500 nM, 16 h) or rapamycin (20 nM, 30 min) prior to insulin (Left) or with tunicamycin (2 μg/mL) for 4, 8 or 16 h (Right). Insulin response quantified in Figure 1—figure supplement 1.

(C) Venn diagram depicting number and overlap of mTORC1- and ISR-induced transcripts, including those increased with insulin (red), decreased relative to insulin with rapamycin (green), and increased with 4 h tunicamycin (orange), and those dependent on ATF4 within these categories (purple), all with *P*-values < 0.05. Only 61 ATF4-dependent genes overlap between those significantly induced by insulin in a rapamycin-sensitive manner and those induced by tunicamycin. Gene lists per category are provided in supplementary table 1.

(D) KEGG enrichment of the shared mTORC1- and ISR-induced ATF4 target genes. *P* values provided were false discovery rate corrected (FDR).

(E) Plot of -$\log_{10}$ *P*-values of 774 ATF4-dependent tunicamycin-induced genes. ATF4-dependent genes induced by both mTORC1 signaling and tunicamycin treatment (shared ISR and mTORC1) are shown in red.

(F) The 61 ATF4-dependent genes induced by both mTORC1 (i.e., rapamycin-sensitive insulin stimulation) and tunicamycin treatment are shown ranked from left to right in order of greatest $\log_2$-fold change with insulin (red bars), with the corresponding tunicamycin-induced changes superimposed (white bars) (n = 4). Error bars depict 95% confidence intervals.

to ATF4 induction by the ISR. Among the 61 shared ATF4-dependent transcripts, those involved in amino acid synthesis and transport, one-carbon metabolism, and aminoacyl tRNA charging often displayed comparable fold-changes between insulin stimulation and tunicamycin treatment, while canonical genes of the ER stress response, such as *Herpud1* and *Ddit3/Chop,* showed much greater induction with tunicamycin (Figure 1F). In addition to aminoacyl tRNA synthetase genes, expression of the *Xpot* gene encoding Exportin-T, which is the major Ran GTPase family member for nuclear to cytosolic export of mature tRNAs (Arts et al., 1998; Kutay et al., 1998), was found to be similarly regulated by ATF4 in response to mTORC1 and ISR activation. Transcripts encoding known negative regulators of mTORC1 signaling are also among these 61 shared ATF4-induced genes, including *Ddit4/Redd1* and *Sesn2* (J. Brugarolas et al., 2004; Condon et al., 2021; Lee et al., 2010; Reiling & Hafen, 2004; Wolfson et al., 2016). These targets likely contribute to the ATF4-dependent inhibition of mTORC1 signaling (S6K1 phosphorylation) observed upon tunicamycin treatment (Figure 1B), while in the context

189 of mTORC1 signaling, these ATF4 targets might play a role in negative feedback
190 regulation of mTORC1. These data suggest that a specific subset of ATF4-dependent
191 ISR-induced genes are likewise regulated by growth factor signaling through mTORC1
192 and are enriched for specific processes including aminoacyl tRNA synthesis, amino acid
193 synthesis and uptake, and one-carbon metabolism.
194
195 ATF4 is known to form heterodimers with other bZIP transcription factors to engage its
196 gene targets, while also co-regulating genes with transcription factors that bind additional
197 promoter elements (Kilberg et al., 2009; Newman & Keating, 2003; Wortel et al., 2017).
198 Thus, we used bioinformatic tools to determine whether the promoters of ATF4 gene
199 targets shared between the ISR and mTORC1 signaling might be distinct from those
200 induced by the ISR alone. Indeed, CiiiDER analysis (Gearing et al., 2019) revealed that
201 there are predicted promoter-binding sequences that distinguish the 61 shared target
202 genes from the top 200 ATF4-dependent genes induced by the ISR alone (Figure 2A—
203 supplementary table 2). Regulatory elements for the C/EBP family of transcription factors,
204 which are well established to heterodimerize with ATF4 to induce its canonical
205 downstream targets (Cohen et al., 2015; Ebert et al., 2020; Huggins et al., 2015), were
206 the most enriched in the promoters of ATF4 gene targets with shared regulation. On the
207 other hand, binding elements for the TEAD family of transcription factors, which function
208 with YAP/TAZ in the Hippo signaling pathway, were enriched in the promoters of ATF4-
209 dependent gene targets significantly induced only by tunicamycin, consistent with
210 published work indicating a functional connection between the unfolded protein response
211 (UPR) and YAP-TEAD activation (Wu et al., 2015; Xiao et al., 2019). We next analyzed
212 the 61 ATF4-dependent genes with shared regulation for physical evidence of promoter
213 binding of specific transcription factors using the Cistrome Data Browser, a portal for
214 mining existing chromatin immunoprecipitation-DNA sequencing (ChIP-Seq) data (Mei et
215 al., 2017; Zheng et al., 2019). Importantly, this second unbiased analysis also revealed
216 C/EBP isoforms as most commonly binding to the promoters of these genes (Figure 2B).
217
218 As all members of the C/EBP family have the potential to heterodimerize with ATF4 and
219 contritbute to the induction of these gene targets (Newman & Keating, 2003), we first

Figure 2

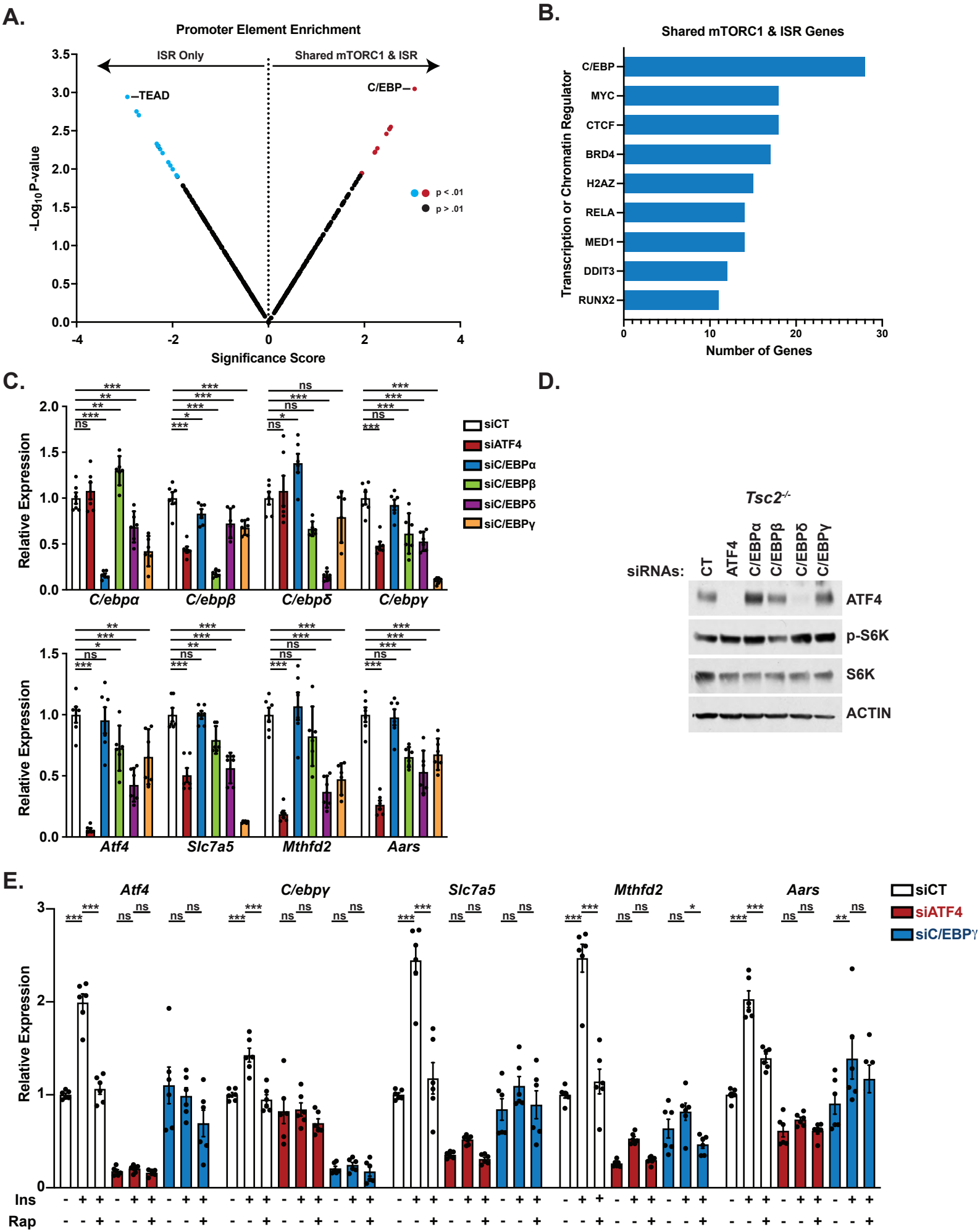
A.
Promoter Element Enrichment
ISR Only
Shared mTORC1 & ISR
TEAD
C/EBP
p < .01
p > .01
-Log10 P-value
Significance Score
B.
Shared mTORC1 & ISR Genes
Transcription or Chromatin Regulator
C/EBP
MYC
CTCF
BRD4
H2AZ
RELA
MED1
DDIT3
RUNX2
Number of Genes
C.
Relative Expression
siCT
siATF4
siC/EBPα
siC/EBPβ
siC/EBPδ
siC/EBPγ
C/ebpα
C/ebpβ
C/ebpδ
C/ebpγ
Atf4
Slc7a5
Mthfd2
Aars
D.
Tsc2-/-
siRNAs:
CT
ATF4
C/EBPα
C/EBPβ
C/EBPδ
C/EBPγ
ATF4
p-S6K
S6K
ACTIN
E.
Atf4
C/ebpγ
Slc7a5
Mthfd2
Aars
siCT
siATF4
siC/EBPγ
Relative Expression
Ins
Rap

220 **Figure 2. C/EBP family transcription factors contribute to the regulation of ATF4-**
221 **dependent genes shared between mTORC1 signaling and the ISR.**
222 (A) CiiiDER analysis comparing transcription factor-binding elements enriched in the
223 promoters of the top 200 ATF4-dependent genes induced by tunicamycin but not insulin
224 (ISR Only) versus the 61 ATF4-dependent genes induced by both mTORC1 signaling
225 and tunicamycin (Shared ISR and mTORC1). Those sequence elements significantly
226 enriched (P<0.01) are shown in blue or red. Data are provided in supplementary table 2.
227 (B) CISTROME analysis of genome-wide ChIP studies to identify transcription factors
228 found to bind to the promoters of the ATF4-dependent genes shared in their regulation
229 by the mTORC1 and the ISR.
230 (C) qPCR analysis of the indicated transcripts in *Tsc2*$^{-/-}$ MEFs transfected with control
231 siRNAs (siCT) or those targeting *Atf4, C/EBP*α*, C/EBP*β*, C/EBP*δ*, C/EBP*γ. Expression
232 relative to siCT for each gene is graphed as mean ± SEM from two independent
233 experiments, each with 3 biological replicates (n=6).
234 (D) Immunoblots of cells treated as in (C).
235 (E) qPCR analysis of the indicated transcripts in serum-deprived WT MEFs treated with
236 insulin (500 nM, 16 h) after 30-min pretreatment with vehicle or rapamycin (20 nM)
237 following transfection with control siRNAs (siCT) or those targeting *Atf4* or *C/ebp*γ.
238 Expression relative to siCT for each gene is graphed as mean ± SEM from two
239 independent experiments, each with 3 biological replicates (n=6). $p < 0.05$, $^{**}p < 0.01$,
240 $^{***}p < 0.001$, ns = not significant. One-way ANOVA with Holm-Sidak method for multiple
241 comparisons was used to determine statistical significance for (C,E).
242

243 determined the effects of siRNA-mediated knockdown of individual isoforms, relative to
244 ATF4 knockdown, on expression of three representative genes in *Tsc2*$^{-/-}$ MEFs, which
245 exhibit growth factor-independent activation of mTORC1 signaling. This analysis revealed
246 that knockdown of ATF4, C/EBPβ, C/EBPδ, or C/EBPγ each led to decreased transcript
247 levels of the shared mTORC1 and ISR gene targets *Slc7a5*, *Mthfd2*, and *Aars* (Figure
248 2C). However, this analysis was complicated by the finding of substantial co-dependence
249 for expression among these bZIP transcription factors, with knockdown of any one of the
250 C/EBP family members or ATF4 significantly changing expression of at least one other
251 family member. C/EBPδ knockdown, for instance, decreased expression of all genes
252 measured, including ATF4, which was also reflected in loss of ATF4 protein (Figure 2C-
253 D). It is worth noting that we were unable to identify reliable antibodies to specific C/EBP
254 family members for use in MEFs. Among C/EBP family members, C/EBPγ has been found
255 in other settings to regulate many of the genes revealed in our analysis to be induced
256 through shared regulation of ATF4 (Huggins et al., 2015), and its knockdown signicantly
257 decreased expression of the three ATF4 target genes tested without effects on ATF4

258 protein levels (Figure 2C-D). Based on this finding, we knocked down ATF4 or C/EBPγ
259 in wild-type MEFs and stimulated the cells with insulin in the presence or absence of
260 rapamycin to determine whether C/EBPγ impacted the mTORC1 and ATF4-dependent
261 regulation of these genes. Indeed, knockdown of C/EBPγ attenuated the insulin-induced
262 expression of these genes, albeit to a lesser extent than ATF4 knockdown (Figure 2E).
263 C/EBPγ knockdown also blocked the ability of insulin to increase ATF4 transript levels,
264 suggesting that following the induction of ATF4 mRNA translation downstream of
265 mTORC1 (Ben-Sahra et al., 2016; Park et al., 2017), it stimulates its own expression via
266 ATF4-C/EBPγ heterodimers. Thus, C/EBPγ and likely other ATF4-binding partners of the
267 C/EBP family contribute to the induction of ATF4 gene targets following mTORC1-
268 mediated activation of ATF4.
269
270 **mTORC1 signaling induces genes involved in amino acid synthesis, transport, and**
271 **tRNA charging through ATF4 activation**
272 To validate and expand the findings from the RNA-seq analysis, a Nanostring codeset
273 was designed to simultaneously quantify transcripts of genes involved in the enriched
274 processes above (see methods). As positive and negative controls, respectively, we
275 included the glycolytic targets of HIF1, established previously to be regulated downstream
276 of mTORC1 (Duvel et al., 2010), and the mitochondrial tRNA synthetases, not believed
277 to be regulated by ATF4. Using this codeset, we analyzed gene expression in three
278 settings of mTORC1 activation: 1) wild-type MEFs stimulated with insulin in the presence
279 or absence of rapamycin, 2) growth factor-independent activation of mTORC1 via genetic
280 loss of the TSC protein complex in *Tsc2*$^{-/-}$ MEFs, and 3) *Tsc2*$^{-/-}$ MEFs with siRNA-
281 mediated knockdown of ATF4 (Figure 3A—supplementary table 3). ATF4 protein levels
282 were robustly upregulated with either genetic or insulin-stimulated mTORC1 activation in
283 these settings, with both rapamycin and ATF4-targeting siRNAs blocking this induction
284 (Figure supplement 2A). Interestingly, the majority of transcripts analyzed in the functional
285 categories that encode enzymes of non-essential amino acid synthesis, one-carbon
286 metabolism, amino acid transporters, and cytosolic amino-acyl tRNA synthetases (and
287 *Xpot*) were increased with mTORC1 activation in a manner sensitive to both rapamycin
288 and siRNA-mediated knockdown of ATF4. However, the HIF1 targets of glycolysis were

Figure 3

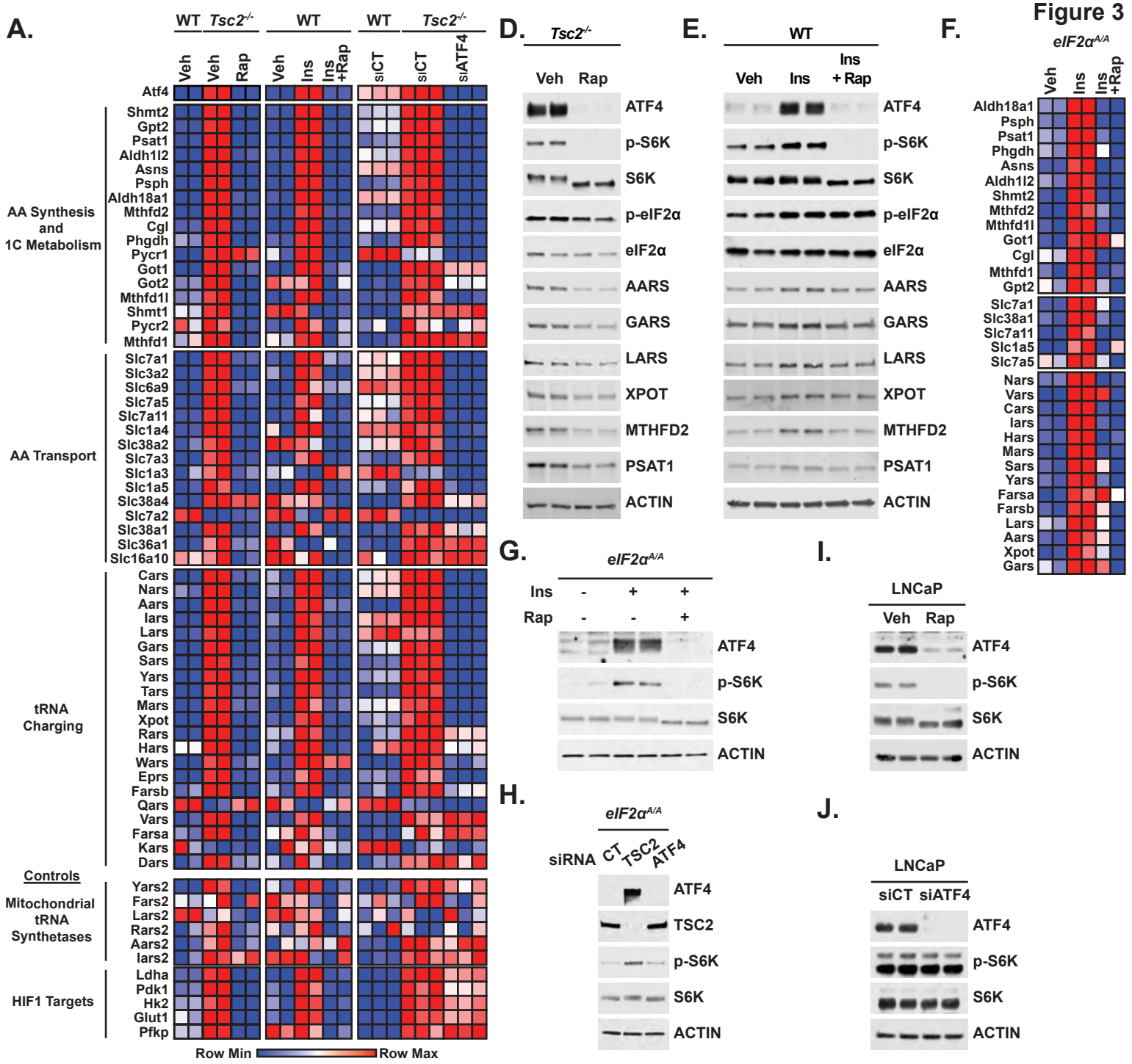
A.
WT
Tsc2-/-
WT
WT
Tsc2-/-
Veh
Veh
Rap
Veh
Ins
Ins +Rap
siCT
siCT
siATF4
Atf4
AA Synthesis and 1C Metabolism
Shmt2
Gpt2
Psat1
Aldh1l2
Asns
Psph
Aldh18a1
Mthfd2
Cgl
Phgdh
Pycr1
Got1
Got2
Mthfd1l
Shmt1
Pycr2
Mthfd1
AA Transport
Slc7a1
Slc3a2
Slc6a9
Slc7a5
Slc7a11
Slc1a4
Slc38a2
Slc7a3
Slc1a3
Slc1a5
Slc38a4
Slc7a2
Slc38a1
Slc36a1
Slc16a10
tRNA Charging
Cars
Nars
Aars
Iars
Lars
Gars
Sars
Yars
Tars
Mars
Xpot
Rars
Hars
Wars
Eprs
Farsb
Qars
Vars
Farsa
Kars
Dars
Controls
Mitochondrial tRNA Synthetases
Yars2
Fars2
Lars2
Rars2
Aars2
Iars2
HIF1 Targets
Ldha
Pdk1
Hk2
Glut1
Pfkp
Row Min
Row Max
D.
Tsc2-/-
Veh
Rap
ATF4
p-S6K
S6K
p-eIF2α
eIF2α
AARS
GARS
LARS
XPOT
MTHFD2
PSAT1
ACTIN
E.
WT
Veh
Ins
Ins + Rap
ATF4
p-S6K
S6K
p-eIF2α
eIF2α
AARS
GARS
LARS
XPOT
MTHFD2
PSAT1
ACTIN
F.
eIF2αA/A
Veh
Ins
Ins +Rap
Aldh18a1
Psph
Psat1
Phgdh
Asns
Aldh1l2
Shmt2
Mthfd2
Mthfd1l
Got1
Cgl
Mthfd1
Gpt2
Slc7a1
Slc38a1
Slc7a11
Slc1a5
Slc7a5
Nars
Vars
Cars
Iars
Hars
Mars
Sars
Yars
Farsa
Farsb
Lars
Aars
Xpot
Gars
G.
eIF2αA/A
Ins - + +
Rap - - +
ATF4
p-S6K
S6K
ACTIN
I.
LNCaP
Veh
Rap
ATF4
p-S6K
S6K
ACTIN
H.
eIF2αA/A
siRNA CT TSC2 ATF4
ATF4
TSC2
p-S6K
S6K
ACTIN
J.
LNCaP
siCT siATF4
ATF4
p-S6K
S6K
ACTIN
B.
Relative Expression
Veh WT
Veh
Rap Tsc2-/-
Atf4
Psat1
Mthfd2
Slc7a5
Aars
Gars
C.
Relative Expression
Veh
Ins
Ins + Rap
Atf4
Psat1
Mthfd2
Slc7a5
Aars
Gars
K.
Relative Expression
LNCaP
Veh
Rap
ns
PSAT1
ASNS
MTHFD2
SLC7A5
AARS
GARS
XPOT
L.
Relative Expression
LNCaP
siCT
siATF4
PSAT1
ASNS
MTHFD2
SLC7A5
AARS
GARS
XPOT

Figure 3. mTORC1 and ATF4 regulate genes involved in amino acid synthesis, transport, and tRNA charging.

(A) Row-normalized heatmaps of Nanostring gene expression data are shown from 1) serum-deprived wild-type (WT) or *Tsc2*$^{-/-}$ MEFs treated (16 h) with vehicle (Veh) or rapamycin (20 nM, Rap) (n=2), 2) serum-deprived WT MEFs treated with insulin (500 nM, 16 h, Ins) following 30-min pretreatment with vehicle or rapamycin (20 nM) (n=2), and 3) WT and *Tsc2*$^{-/-}$ MEFs transfected with *Atf4* siRNAs or non-targeting controls (siCT) and serum-deprived for 16 h (n=3). Genes are grouped by functional category and ranked in order of most significantly decreased with ATF4 knockdown for each group. Heatmap values are provided in supplementary table 3, and effects on ATF4 protein levels and mTORC1 signaling for each condition are shown by immunoblot in supplemental Figure S2A.

(B,C) qPCR analysis of the indicated transcripts in WT and *Tsc2*$^{-/-}$ MEFs (B) or WT MEFs stimulated with insulin in the presence or absence of rapamycin (C) as in (A). Expression relative to vehicle-treated, unstimulated WT cells is graphed as mean ± SEM from three independent experiments, each with 3 biological replicates (n=9). Effects of ATF4 knockdown are shown in supplemental Figure 3—figure supplement 2B.

(D,E) Representative immunoblots of *Tsc2*$^{-/-}$ MEFs treated with vehicle or rapamycin as in (A) or serum-deprived WT MEFs stimulated with insulin (500 nM, 24 h) following 30-min pretreatment with vehicle or rapamycin (20 nM), with biological duplicates shown for each condition. Quantification provided in Figure 3—figure supplement 2C,D.

(F) Row-normalized heatmaps of Nanostring gene expression data for transcripts in the functional groups from (A) found to be significantly ($p < 0.05$) induced in *eIF2*$\alpha^{A/A}$ MEFs treated with insulin (500 nM, 16h) following 30-min pretreatment with vehicle or rapamycin (20 nM) (n=2). Genes are ranked by category in order of most significantly increased with insulin for each group. The heatmap values are provided in supplementary table 3. Immunoblots validating that these cells are defective in the ISR and qPCR validation of representative genes are provided in Figure 3—figure supplement 2E,F.

(G) Representative immunoblot of cells treated as in (F), with biological duplicates shown for each condition.

(H) Representative immunoblot of *eIF2*$\alpha^{A/A}$ MEFs transfected with siRNAs targeting *Atf4, Tsc2,* or non-targeting controls (CT) prior to serum-starvation for 16 h.

(I,J) Representative immunoblot of serum-deprived LNCaP cells treated with vehicle or rapamycin (20 nM, 16 h) (I) or *Atf4* siRNAs versus non-targeting controls (siCT) (J), with biological duplicates shown for each.

(K,L) qPCR analysis of the indicated transcripts in LNCaP cells serum-starved in the presence of vehicle or rapamycin (20 nM, 16 h) (K) or transfected with *ATF4* siRNAs or non-targeting controls (siCT) and serum-starved for 16 h (L). Expression relative to vehicle-treated cells is graphed as mean ± SEM from two independent experiments, with 3 biological replicates each (n=6). Immunoblots and qPCR analysis for PC3 cells treated as in (I-L) are provided in Figure 3—figure supplement 2G-J, and effects of c-Myc knockdown on representative gene targets is shown in supplemental Figure 3—figure supplement 2K,L.

*$p < 0.05$, **$p < 0.01$, ***$p < 0.001$, ns = not significant. One-way ANOVA with Holm-Sidak method for multiple comparisons was used to determine statistical significance for (B,C).

334 Unpaired two-tailed t-test was used to determine statistical significance for (F,K,L).
335 (D,E,G,H,I,J) are representative of at least two independent experiments.
336

337 mTORC1-regulated but independent of ATF4, and transcripts encoding the mitochondrial
338 tRNA synthetases were reproducibly regulated by neither mTORC1- nor ATF4. We
339 further confirmed the mTORC1- and ATF4-mediated regulation of a representative subset
340 of these transcripts via qPCR (Figure 3B-C—figure supplement 2B). Consistent with
341 previous studies (Ben-Sahra et al., 2016; Park et al., 2017), both ATF4 transcript and
342 protein levels were induced by mTORC1 signaling in these settings (Figure 3B-E).
343 Transcriptional changes in ATF4 gene targets were reflected in corresponding changes
344 in the abundance of representative protein products, with varying degrees of rapamycin
345 sensitivity, likely reflecting inherent differences in the turnover rates of these proteins
346 (Figure 3D-E, quantified in figure supplement 2C-D). We next wanted to confirm that
347 these mTORC1- and ATF4-induced changes were independent of the ISR. While we
348 have shown previously that mTORC1 regulates ATF4 in a manner that is independent of
349 eIF2α-S51 phosphorylation (Ben-Sahra et al., 2016), chronic activation of mTORC1 upon
350 loss of TSC2 is known to cause a basal increase in ER stress and activation of the ISR
351 (Ozcan et al., 2008). Therefore, we utilized MEFs with endogenous, homozygous knock-
352 in of the *eIF2α-S51A* mutation (*eIF2$\alpha^{A/A}$*), which fail to induce ATF4 downstream of
353 cellular stress (Figure supplement 2E) (Scheuner et al., 2001). Consistent with mTORC1-
354 dependent, ISR-independent regulation, insulin increased ATF4 protein levels and
355 expression of its gene targets involved in amino acid synthesis and one-carbon
356 metabolism, amino acid transporters, and amino-acyl tRNA synthetases in a rapamycin
357 sensitive manner in these cells, as shown by Nanostring analysis and confirmed for a
358 subset of genes by qPCR (Figure 3F-G—figure supplement 2F). Notably, like insulin
359 stimulation, genetic activation of mTORC1 via siRNA-mediated knockdown of *Tsc2* in the
360 *eIF2$\alpha^{A/A}$* MEFs also increased ATF4 protein levels, further confirming that this regulation
361 can occur independent of the ISR (Figure 3H). Growth factor-independent activation of
362 mTORC1 also occurs upon loss of the PTEN tumor suppressor, and rapamycin was found
363 to decrease ATF4 protein levels and ATF4-dependent expression of representative gene
364 targets in established PTEN-deficient prostate cancer cells, LNCaP and PC3 (Figure 3I-
365 L—figure supplement 2G-J).

366 The transcription factor c-MYC can be activated downstream of mTORC1 in some
367 settings and has previously been shown to regulate many of the same ATF4 target genes
368 encoding the enzymes of amino acid synthesis and transport, as well as amino-acyl tRNA
369 synthetases (Csibi et al., 2014; Stine et al., 2015; Wall et al., 2008; Zirin et al., 2019). A
370 survey of expression for 11 of such genes in *Tsc2*$^{-/-}$ cells finds that the majority are not
371 significantly affected by siRNA-mediated knockdown of c-MYC, whereas a few others are
372 modestly but significantly decreased (e.g., *Gars*, *Slc1a5*, *Psat1*), albeit to a lesser degree
373 than with siRNA-mediated knockdown of ATF4 (Figure 3—figure supplement 2K-L).
374
375 To determine whether ATF4 activation is both necessary and sufficient for mTORC1-
376 mediated regulation of these gene targets related to amino acid acquisition and utilization,
377 we knocked out *Atf4* using CRISPR/Cas9 in *Tsc2*$^{-/-}$ MEFs and confirmed biallelic
378 disruption (Figure 4A). Protein levels of identified ATF4 targets were decreased in *Tsc2*$^{-}$
379 $^{/-}$ *Atf4*$^{-/-}$ MEFs and fully rescued with expression of wild-type ATF4 but not a DNA-binding
380 domain mutant (ATF4^{DBD}) (Figure 4B). As mTORC1 regulates ATF4 translation through
381 a mechanism requiring its 5'-UTR (Ben-Sahra et al., 2016; Park et al., 2017), the stably
382 rescued cell lines, which express an ATF4 cDNA lacking the 5' UTR, exhibit protein
383 expression of ATF4 and its encoded gene targets that are resistant to rapamycin (Figure
384 4C—figure supplement 3). The expression of select ATF4 target transcripts were
385 markedly decreased in *Tsc2*$^{-/-}$ *Atf4*$^{-/-}$ MEFs, to a similar extent to that measured in *Atf4*
386 wild-type cells treated with rapamycin (Figure 4D). These transcript levels were rescued
387 with the expression of wild-type ATF4, but not ATF4^{DBD}, in a manner that was completely
388 or partially rapamycin resistant (Figure 4D). These collective data show that mTORC1
389 signaling drives the expression of genes involved in tRNA export and charging, amino
390 acid uptake, and non-essential amino acid synthesis through its downstream regulation
391 of the ATF4 transcription factor.
392
393 **Activation of ATF4 contributes to the induction of protein synthesis downstream**
394 **of mTORC1**
395 mTORC1 induces protein synthesis through multiple downstream targets (Valvezan &
396 Manning, 2019). Given that the major mTORC1-regulated ATF4 target genes identified

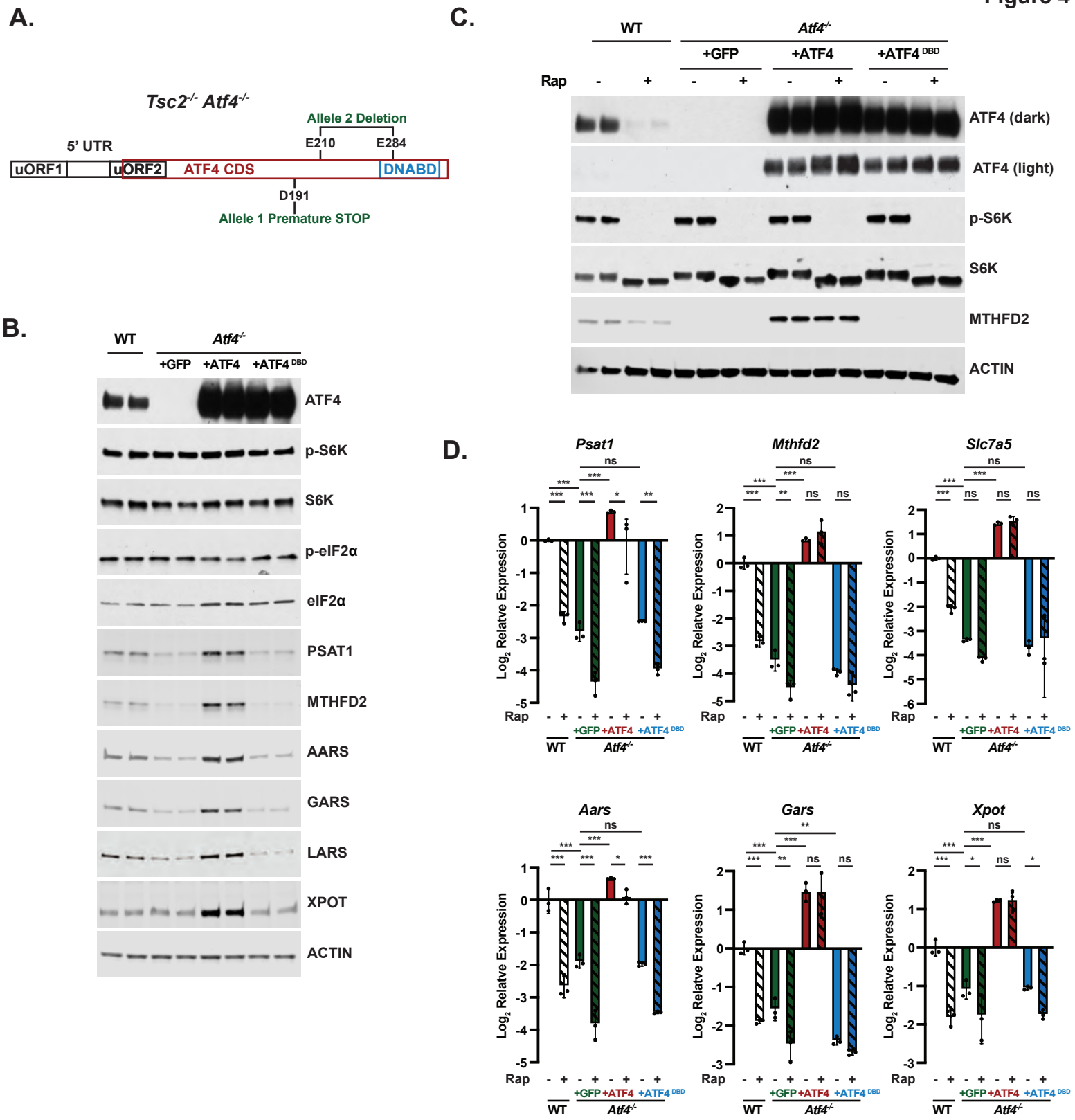

Figure 4. Use of ATF4 knockout cells and a rapamycin-resistant ATF4 to validate ATF4 targets regulated by mTORC1 signaling.

(A) Schematic of ATF4 transcript, including upstream open reading frames (uORFs), coding sequence (CDS), and DNA-binding domain (DNABD), highlighting location of CRISPRn guides biallelic location of ATF4 mutations generated in *Tsc2*$^{-/-}$ MEFs.

(B,C) Representative immunoblots of serum-deprived *Tsc2*$^{-/-}$ (WT) MEFs or *Tsc2*$^{-/-}$ *Atf4*$^{-/-}$ MEFs with stable expression of cDNAs encoding GFP, ATF4 lacking its 5'UTR, or a

404 DNABD mutant (DBD) of this ATF4 left untreated (B) or treated with vehicle or rapamycin
405 (20 nM, 16h) (C), with biological duplicates shown for each condition. Immunoblots of
406 proteins encoded by ATF4 gene targets in these cells are provided in Figure supplement
407 3.
408 (D) qPCR analysis of the indicated transcripts from cells treated as in (C). Expression
409 relative to WT vehicle-treated cells is graphed as the $\log_2$ mean ± SD from a
410 representative experiment with three biological replicates (n=3). *p < 0.05, **p < 0.01, ***p
411 < 0.001, ns = not significant, calculated via one-way ANOVA with Holm-Sidak method for
412 multiple comparisons.
413 (B-D) are representative of at least two independent experiments.
414

415 above are involved in amino acid uptake, synthesis, and tRNA charging, we hypothesized
416 that ATF4 induction through mTORC1 signaling might contribute to the canonical
417 increase in protein synthesis upon mTORC1 activation. Relative rates of protein synthesis
418 were measured via [^{35}S]-methionine incorporation into newly synthesized proteins in
419 *Tsc2*$^{+/+}$ and *Tsc2*$^{-/-}$ cells treated with control siRNAs or *Tsc2*$^{-/-}$ cells treated with siRNAs
420 targeting ATF4 or Rheb, the small GTPase target of TSC2 that is an essential upstream
421 activator of mTORC1. siRNA-mediated knockdown of either ATF4 or Rheb substantially
422 decreased ATF4 protein levels in *Tsc2*$^{-/-}$ cells (Figure 5A). Importantly, the elevated rate
423 of protein synthesis in *Tsc2*$^{-/-}$ MEFs was decreased with ATF4 knockdown to a similar
424 extent to that observed with Rheb knockdown (Figure 5A,B). No change in mTORC1
425 signaling or phosphorylation of eIF2α was observed with ATF4 knockdown in this setting
426 (Figure 4A—figure supplement 4A). Protein synthesis was also measure in the *Tsc2*$^{-/-}$
427 *Atf4*$^{-/-}$ cell lines described above. Notably, the cells lacking ATF4 exhibited increased
428 uptake of [^{35}S]-methionine relative to parental cells and those reconstituted with ATF4
429 (Figure supplement 4B). Despite this unexplained difference in methionine uptake, *Atf4*
430 knockout cells exhibited a reduced rate of protein synthesis that was similar to the
431 parental lines treated with rapamycin (Figure 5C,D). However, rapamycin treatment
432 further reduced protein synthesis in the *Atf4* knockout cells. Importantly, cells
433 reconstituted with the rapamycin-resistant ATF4 cDNA exhibited rescued protein
434 synthesis, surpassing that observed in cells with endogenous ATF4, but this enhanced
435 protein synthesis was still significantly reduced with rapamycin. Like *Tsc2*$^{-/-}$ cells, wild-
436 type cells cultured in the presence of growth factors exhibited reduced protein synthesis
437 upon deletion of *Atf4*, again with a reduction similar to that from rapamycin treatment

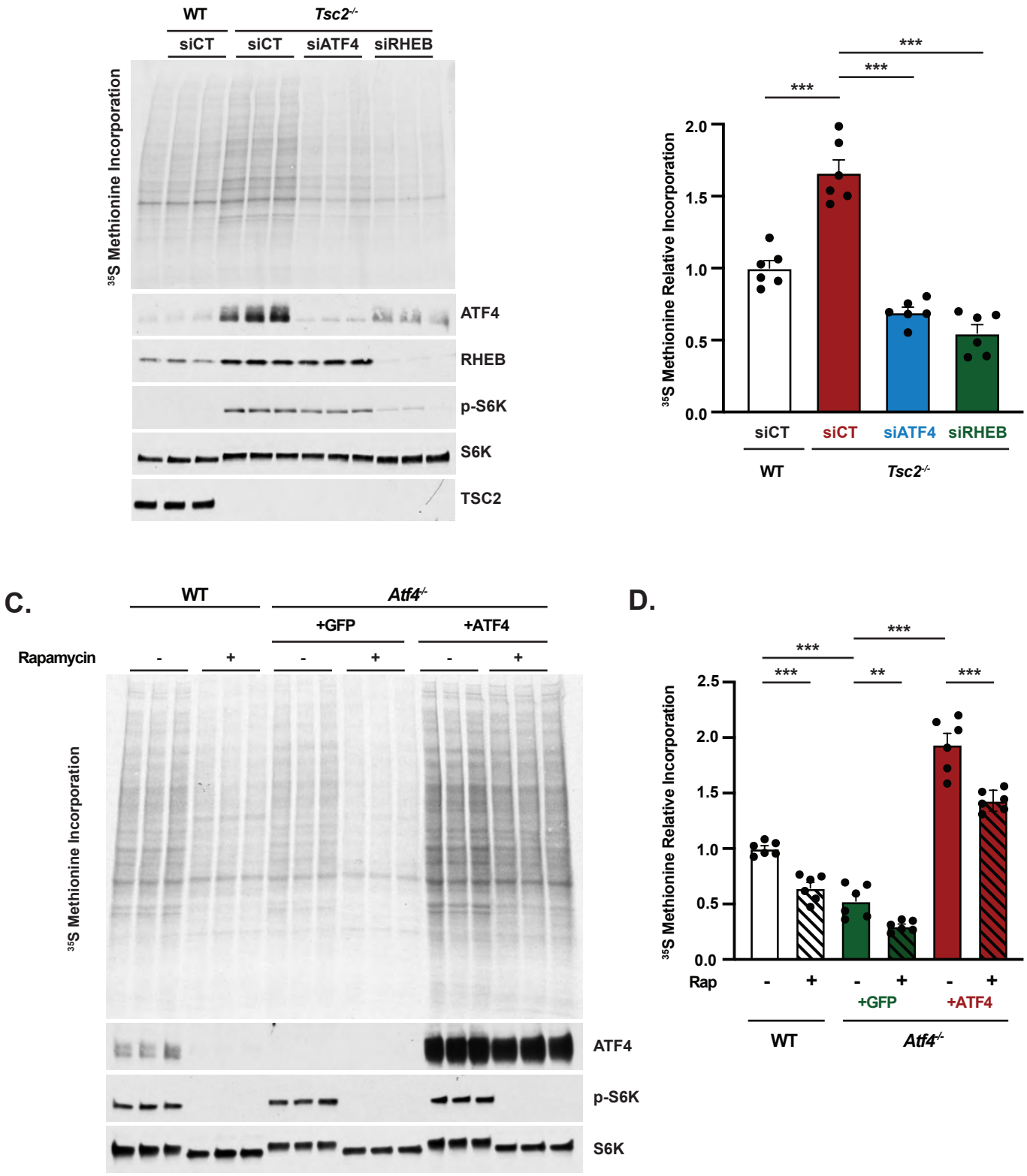

Figure 5. Activation of ATF4 contributes to the induction of protein synthesis downstream of mTORC1.

(A, B) Representative autoradiogram and immunoblot of WT and *Tsc2*$^{-/-}$ MEFs transfected with siRNAs targeting *Atf4* or *Rheb1* and *Rhebl1* or non-targeting controls (siCT) and serum-deprived for 16 h with a pulse label of [^{35}S]-methionine for the final 20 min (A) and quantified in (B). Biological triplicates from a representative experiment are shown in (A).

444 (B) is graphed as mean ± SEM from two independent experiments, each with 3 biological
445 replicates (n=6). Lack of effect of ATF4 knockdown on eIF2α phosphorylation is shown
446 in supplemental Figure 5—figure supplement 4A.
447 (C,D) Representative autoradiogram and immunoblot of serum-deprived *Tsc2*$^{-/-}$ MEFs
448 (WT) or *Tsc2*$^{-/-}$ *Atf4*$^{-/-}$ MEFs with stable expression of cDNAs encoding GFP or ATF4
449 lacking its 5'UTR treated with vehicle or rapamycin (20 nM, 16 h) with a pulse label of
450 [^{35}S]-methionine for the final 20 min (C) and quantified in (D). Biological triplicates from a
451 representative experiment are shown in (C). (D) is graphed as mean ± SEM from two
452 independent experiments, each with 3 biological replicates (n=6). Measurement of
453 methionine uptake in these cells is provided in Figure 5—figure supplement 4B, and
454 effects of ATF4 knockout on protein synthesis in growth-factor stimulated wild-type MEFs
455 are shown in Figure 5—figure supplement 4C,D.
456 (B,D) *$p < 0.05$, **$p < 0.01$, ***$p < 0.001$, ns = not significant, calculated via one-way
457 ANOVA with Holm-Sidak method for multiple comparisons.
458

459 (Figure 5—figure supplement 4C-D). Together, these data suggest that ATF4 induction
460 downstream of mTORC1 is necessary but not sufficient for mTORC1-regulated protein
461 synthesis, consistent with the multiple mechanisms through which mTORC1 controls this
462 key anabolic process.
463

464 **mTORC1 regulates cystine uptake through ATF4**

465 Among the 61 shared mTORC1- and ISR-induced ATF4 gene targets identified, the
466 cystine-glutamate antiporter *Slc7a11* was the gene with the highest fold induction by
467 RNA-Seq analysis upon insulin treatment (Figure 1F). SLC7A11 (also known as xCT)
468 associates with SLC3A2 (CD98) at the plasma membrane and serves as the primary
469 transporter of cystine, the oxidized form of cysteine and predominant cysteine species in
470 both plasma and cell culture media, whereas reduced cysteine is transported through
471 neutral amino acid systems (Figure 6A) (Bannai & Kitamura, 1980; Conrad & Sato, 2012).
472 Transcript levels of *Slc7a11* were sensitive to rapamycin in *Tsc2*$^{-/-}$ MEFs and greatly
473 decreased with ATF4 knockout (Figure 6B). Upon reconstitution with rapamycin-resistant
474 ATF4, expression of *Slc7a11* was rescued and no longer sensitive to rapamycin, while
475 the ATF4^{DBD} mutant was unable to restore *Slc7a11* transcript levels. A similar pattern of
476 mTORC1- and ATF4-regulated expression was measured for *Slc3a2* (Figure 6C).
477 SLC7A11 protein, detected using an antibody validated with siRNA knockdown (Figure
478 6—figure supplement 5A), decreased in *Tsc2*$^{-/-}$ MEFs treated with mTOR inhibitors and
479 were increased in wild-type MEFs stimulated with insulin in an mTOR-dependent manner

Figure 6

A.

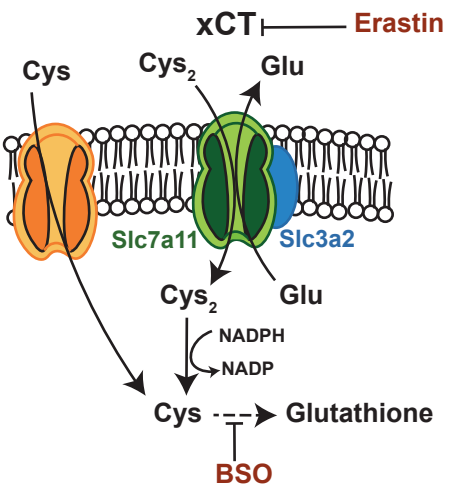

B.

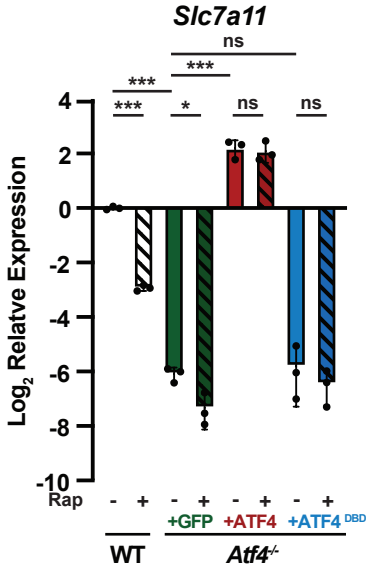

C.

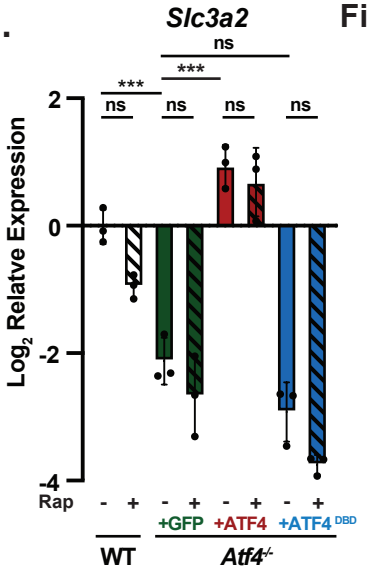

D.

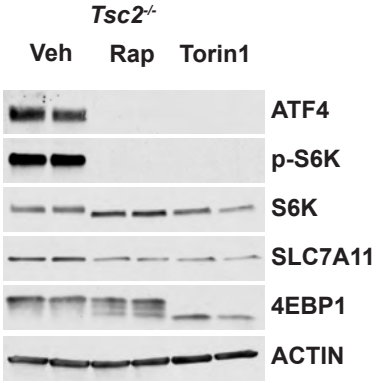

E.

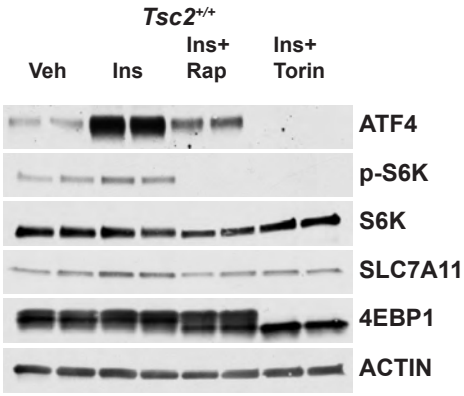

F.

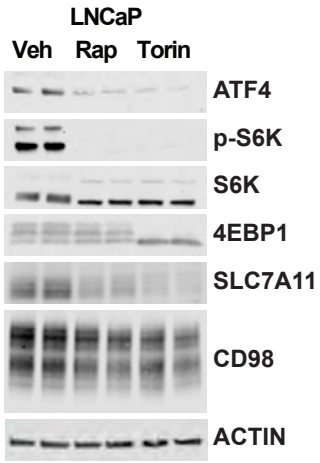

G.

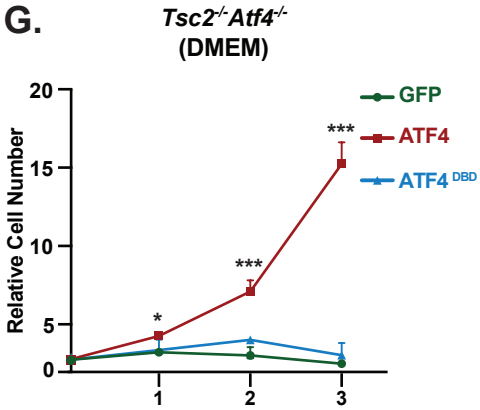

H.

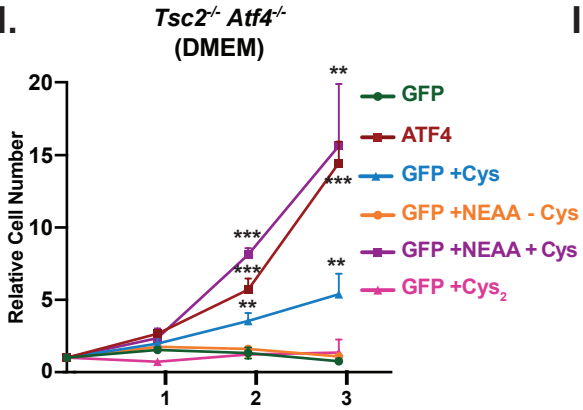

I.

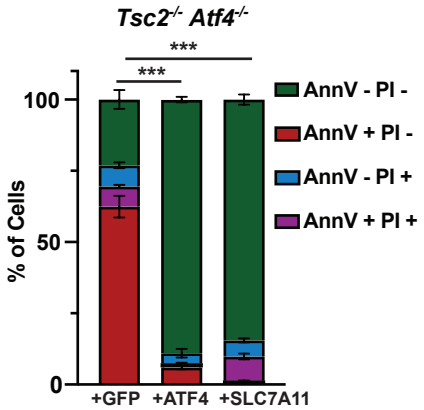

J.

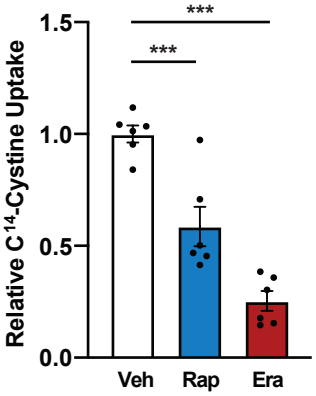

K.

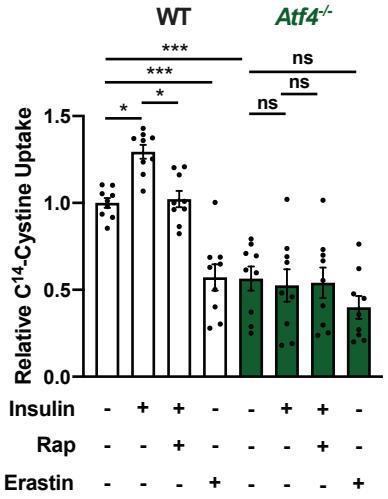

L.

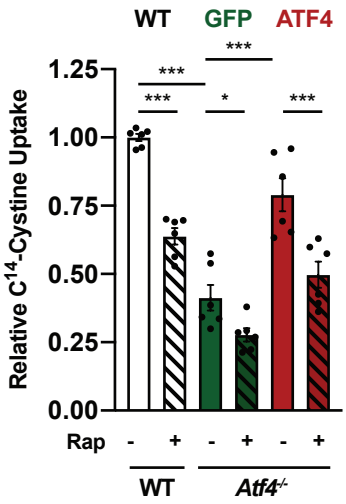

480 **Figure 6. mTORC1 regulates cystine uptake through ATF4 and its target SLC7A11.**
481 (A) Schematic of transporter xCT, encoded by *Slc7a11*, which heterodimerizes with
482 SLC3A2 to serve as a cystine (Cys_2)/glutamate anti-porter. Cystine is reduced to cysteine
483 (Cys), which is essential for glutathione synthesis. Cysteine transport is mediated by
484 neutral amino acid trasporters distict from xCT. The targets of Erastin and BSO, two
485 compounds used in this study, are also depicted.
486 (B,C) qPCR analysis of *Slc7a11* (B) or *Slc3a2* (C) in serum-deprived *Tsc2*$^{-/-}$ MEFs (WT)
487 and *Tsc2*$^{-/-}$ *Atf4*$^{-/-}$ MEFs with stable expression of cDNAs encoding GFP (control), ATF4
488 lacking its 5'UTR, or a DNABD mutant (DBD) of this ATF4 treated with vehicle or
489 rapamycin (20 nM, 16 h). Expression relative to WT vehicle-treated cells is graphed as
490 the log_2 mean ± SD from a representative experiment with three biological replicates
491 (n=3).
492 (D-F) Representative immunoblots of serum-deprived *Tsc2*$^{-/-}$ MEFs (D), insulin-stimulated
493 (500 nM, 24h) wild-type MEFs (E), or serum-deprived LNCaP cells (F) treated 24 h (D,E)
494 or 16 h (F) with vehicle, rapamycin (20 nM), or Torin1 (250 nM), shown with biological
495 duplicates. The SLC7a11 antibody is validated for use in MEFs in supplemental Figure
496 S5A, corresponding immunoblots quantified in supplemental Figures S5B,C,F, effects of
497 ATF4 knockdown and rapamycin on *SLC7A11* transcripts in LNCaP and PC3 cells are
498 shown in supplemental Figures S5D,E, and corresponding immunoblots and protein
499 quantification are provided in Figure 6—figure supplement 5G-H.
500 (G, H) Representative growth curves of *Tsc2*$^{-/-}$ *Atf4*$^{-/-}$ MEFs with stable expression of GFP,
501 ATF4, or ATF4^{DBD} grown in 10% dialyzed FBS with DMEM (G) or DMEM supplemented
502 with cysteine alone (Cys, 1 mM), non-essential amino acids (100 μM each) lacking
503 cysteine (NEAA-Cys), or nonessential amino acids plus either cysteine (1 mM,
504 NEAA+Cys), or cystine (0.5 mM, NEAA+Cys_2) (H). Mean cell numbers ± SD relative to
505 Day 0 are graphed from three biological replicates (n=3).
506 (I) Cell death of *Tsc2*$^{-/-}$ *Atf4*$^{-/-}$ MEFs with stable expression of cDNAs encoding GFP, ATF4
507 or SLC7A11 cultured in DMEM with 10% dialyzed FBS was quantified by Annexin V and
508 PI staining after 72 h and graphed as the mean percentage of total cells ± SD from three
509 biological replicates (n=3).
510 (J) Cystine uptake in serum-deprived *Tsc2*$^{-/-}$ MEFs treated with vehicle, rapamycin (20
511 nM), or erastin (10 μM) for 16h is graphed as the mean ± SEM radiolabel incorporation
512 from C^{14}-cystine over the final 10 min relative to vehicle-treated cells from two
513 independent experiments, with three biological replicates each (n=6). The effect of mTOR
514 inhibitors on cystine uptake in littermate-derived *Rictor*$^{+/+}$ and *Rictor*$^{-/-}$ MEFs, and
515 corresponding immunoblots, are shown in Figure 6—figure supplement 5I-J.
516 (K) Cystine uptake in serum-deprived WT and *Atf4*$^{-/-}$ MEFs pretreated 30 min with vehicle
517 or rapamycin (20 nM) prior to insulin stimulation (500 nM, 24 h) or treated with erastin (10
518 μM, 30') was assayed and graphed as in (J) relative to vehicle-treated WT cells with data
519 from three independent experiments, with three biological replicates each (n=9).
520 (L) Cystine uptake in serum-deprived *Tsc2*$^{-/-}$ MEFs (WT) and*Tsc2*$^{-/-}$ *Atf4*$^{-/-}$ MEFs with
521 stable expression of cDNAs encoding GFP or ATF4 treated with vehicle or rapamycin (20
522 nM) for 16 h was assayed and graphed as in (J) relative to vehicle-treated WT cells with
523 data from two independent experiments, with three biological replicates each (n=6).
524 (B-I) are representative of at least two independent experiments.

525 *p < 0.05, **p < 0.01, ***p < 0.001, ns = not significant, calculated in (B,C,I,J,K,L) via one-
526 way ANOVA with Holm-Sidak method for multiple comparisons and in (G,H) via unpaired
527 two tailed t-test. For (I), the sum of Annexin V+/PI- , Annexin V-/PI+, and Annexin V+/PI+
528 populations were used for comparisons to the Annexin V-/P- population.
529

530 (Figure 6D-E—quantified in figure supplement 5B-C). *SLC7A11* transcript levels were
531 also decreased with both ATF4 knockdown and rapamycin in the PTEN-deficient cancer
532 cell lines LNCaP and PC3, although *SLC7A11* expression was relatively more resistant
533 to rapamycin in PC3 cells (Figure 6—figure supplement 6D-E). SLC7A11 protein levels
534 likewise decreased in LNCaP and PC3 cells treated with mTOR inhibitors, without
535 significant changes to the *SLC3A2* gene product CD98 (Figure 6F—figure supplement
536 5F-H). These data confirm and extend the findings from RNA-Seq and Nanostring
537 analyses (Figure 1F, Figure 3A and 3F) and demonstrate that ATF4 is both necessary
538 and sufficient for the mTORC1-mediated induction of *Slc7a11* expression.
539

540 ATF4 is known to be important for the uptake and synthesis of non-essential amino acids
541 (NEAAs) (Harding et al., 2003). In agreement with this, we observed that *Tsc2*$^{-/-}$ *Atf4*$^{-/-}$
542 cells fail to proliferate in DMEM, which only contains a subset of NEAAs, while addback
543 of wild-type ATF4, but not ATF4^{DBD}, restored proliferation (Figure 6G). Supplementation
544 of DMEM with a mixture of all NEAAs, including cysteine, allowed the *Tsc2*$^{-/-}$ *Atf4*$^{-/-}$ MEFs
545 to proliferate at the same rate as the ATF4-reconstituted cells, while NEAAs lacking
546 cysteine completely failed to support proliferation of these cells (Figure 6H). Furthermore,
547 supplementation with excess reduced cysteine alone, but not equimolar concentrations
548 of oxidized cysteine in the form of cystine, was able to significantly increase proliferation
549 of the *Tsc2*$^{-/-}$ *Atf4*$^{-/-}$ MEFs, albeit to a lesser extent than NEAAs plus cysteine. The majority
550 of these cells die after 72 hours in DMEM, and exogenous expression of either ATF4 or
551 SLC7A11 restores their survival (Figure 6I). Taken together, these data indicate that a
552 defect in the acquisition of cysteine, which normally occurs through SLC7A11-mediated
553 uptake of cystine, underlies the inability of *Tsc2*$^{-/-}$ *Atf4*$^{-/-}$ cells to proliferate or survive in
554 DMEM and suggest a key role for mTORC1 signaling in controlling cystine uptake through
555 ATF4.

556 To directly test whether mTORC1 influences cystine uptake, we employed both genetic
557 (*Tsc2* loss) and physiologic (insulin stimulation) activation of mTORC1, measuring [^{14}C]-
558 cystine uptake in the presence or absence of rapamycin or the xCT inhibitor erastin
559 (Figure 6A) (Yang & Stockwell, 2008). Both rapamycin and erastin significantly decreased
560 [^{14}C]-cystine uptake into *Tsc2*$^{-/-}$ MEFs (Figure 6J). In wild-type MEFs, insulin stimulated
561 an increase in cystine uptake that was inhibited with rapamycin, and this mTORC1-
562 regulated cystine transport was completely lost with ATF4 knockout, reduced to levels of
563 erastin-treated cells (Figure 6K). Additionally, *Tsc2*$^{-/-}$ *Atf4*$^{-/-}$ MEFs showed a decrease in
564 cystine uptake when compared to parental *Tsc2*$^{-/-}$ MEFs, which could be rescued with re-
565 expression of ATF4 (Figure 6L). However, cystine consumption in cells reconstituted with
566 rapamycin-resistant ATF4 was still significantly sensitive to rapamycin treatment,
567 suggesting the existence of additional, ATF4-independent mechanisms influencing the
568 transport or cellular incorporation of cystine downstream of mTORC1. As mTORC2 has
569 been previously suggested to directly regulate xCT (Gu et al., 2017), we utilized *Rictor*$^{-/-}$
570 MEFs, which lack mTORC2 activity, to determine whether mTORC2 was contributing to
571 the decreased cystine uptake observed upon treatment with mTOR inhibitors. While
572 *Rictor*$^{-/-}$ MEFs displayed increased uptake of cystine relative to their wild-type
573 counterparts, cystine uptake, as well as ATF4 protein levels, were sensitive to rapamycin
574 and Torin1 in both cell lines (Figure supplement 5I-J). Thus, mTORC1 promotes cellular
575 cystine uptake, at least in part, through the activation of ATF4 and induction of *Slc7a11*
576 expression, which supports cell proliferation and survival.
577
578 **mTORC1 regulates glutathione levels through ATF4-mediated induction of *Slc7a11***
579 Cysteine, generally acquired through cystine uptake and reduction, is an essential
580 component of the tripeptide glutathione (Figure 6A), the most abundant antioxidant in
581 cells (Meister, 1983). We hypothesized that the regulation of cystine uptake through
582 mTORC1 and ATF4 might influence cellular glutathione content. Indeed, mTORC1
583 inhibition with rapamycin or Torin1 significantly decreased total glutathione levels in *Tsc2*$^{-}$
584 $^{/-}$ MEFs, albeit less than buthionine-sulfoximine (BSO), a direct inhibitor of glutathione
585 synthesis (Figure 7A) (Griffith & Meister, 1979). Similar to BSO treatment, mTOR
586 inhibitors decreased both reduced (GSH) and oxidized (GSSG) forms of glutathione to

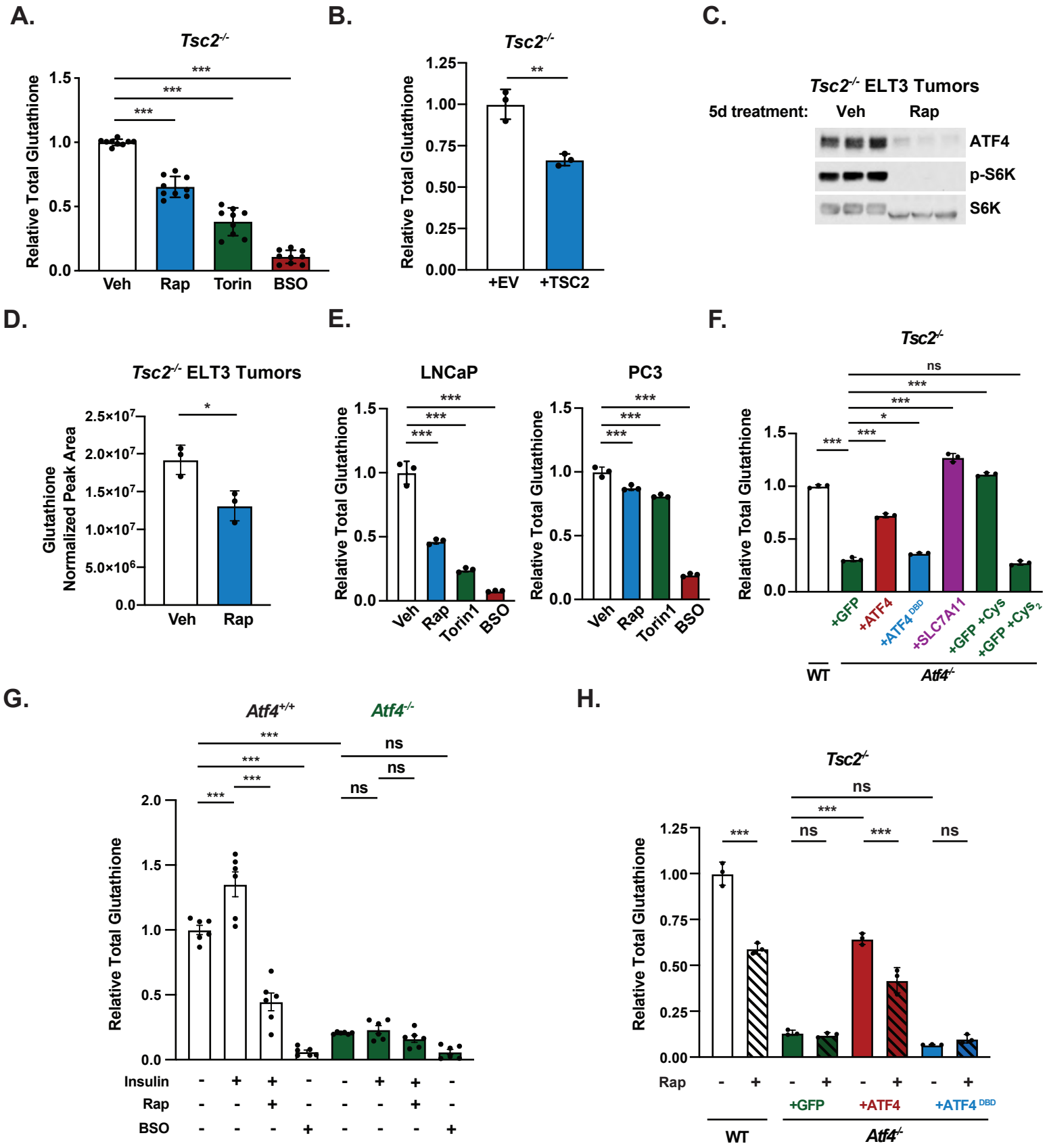

Figure 7. mTORC1 regulates cellular glutathione levels through ATF4 and SLC7A11-mediated cystine uptake.

(A) Total glutathione in serum-deprived *Tsc2*$^{-/-}$ MEFs treated with rapamycin (20 nM), Torin1 (250 nM), or BSO (10 μM) for 16 h is graphed as mean ± SEM relative to vehicle-

591 treated cells from three independent experiments, each with three biological replicates
592 (n=9). Relative abundance of reduced (GSH) and oxidized (GSSG) glutathione from this
593 experiment is shown in supplemental Figure 7—figure supplement 6A.
594 (B) Relative total glutathione in serum-deprived *Tsc2*$^{-/-}$ MEFs with stable reconstitution of
595 a cDNA encoding TSC2 or empty vector (EV) control is graphed as mean ± SD from a
596 representative experiment with three biological replicates (n=3).
597 (C, D) Immunoblot (C) and relative glutathione levels measured by LC-MS/MS (D) from
598 *Tsc2*$^{-/-}$ ELT3 xenograft tumors resected from mice treated for 5 days with vehicle or
599 rapamycin (1 mg/kg on days 1, 3, and 5) (n = 3 mice/group). Relative glutathione levels
600 from rapamycin-treated human *TSC2*$^{-/-}$ tumor cells are shown in Figure 7—figure
601 supplement 6B.
602 (E) Total glutathione in serum-deprived LNCaP (left) and PC3 (right) cells treated with
603 vehicle, rapamycin (20 nM), Torin1 (250 nM), or BSO (50 μM) for 24 h is graphed as
604 mean ± SD relative to vehicle treated cells from a representative experiment with three
605 biological replicates (n=3).
606 (F) Total glutathione in serum-deprived *Tsc2*$^{-/-}$ MEFs (*Atf4* WT) and *Tsc2*$^{-/-}$ *Atf4*$^{-/-}$ MEFs
607 with stable expression of cDNAs encoding GFP (control), ATF4, ATF4^{DBD}, or SLC7A11
608 grown in DMEM and supplemented, where indicated, with cysteine (1 mM, Cys) or cystine
609 (0.5 mM, Cys_2) is graphed as mean ± SD relative to WT cells from a representative
610 experiment with three biological replicates (n=3). Relative glutathione in these cells
611 supplemented with NEAA with or without Cys, measured by LC-MS/MS, is shown in
612 Figure 7—figure supplement 6C.
613 (G) Total glutathione in serum-deprived *Atf4*$^{+/+}$ and *Atf4*$^{-/-}$ MEFs pretreated 30 min with
614 vehicle or rapamycin (20 nM) prior to insulin stimulation (500 nM, 24 h) or treated with
615 BSO (10μM, 24 h) is graphed as mean ± SEM relative to unstimulated Atf4$^{+/+}$ cells from
616 two independent experiments, with 3 biological replicates each (n=6).
617 (H) Total glutathione in serum-deprived *Tsc2*$^{-/-}$ MEFs (*Atf4* WT) and *Tsc2*$^{-/-}$ *Atf4*$^{-/-}$ MEFs
618 with stable expression of cDNAs encoding GFP, ATF4 lacking its 5'UTR, or a DNABD
619 mutant (DBD) of this ATF4 treated with vehicle or rapamycin (20 nM) for 16 h is graphed
620 as mean ± SD relative to vehicle-treated WT cells from a representative experiment with
621 three biological replicates (n=3). Effects of mTORC1 signaling and ATF4 on GCLC and
622 GCLM transcript and protein levels are shown in Figure 7—figure supplement 6D-G.
623 (B, E, F, H) are representative of at least two independent experiments. *$p < 0.05$, **$p <$
624 0.01, ***$p < 0.001$, ns = not significant, calculated in (A,E,F,G,H) via one-way ANOVA
625 with Holm-Sidak method for multiple comparisons and in (B,D) via unpaired two tailed t-
626 test.
627

628 the same degree, indicating effects on total glutathione abundance rather than its redox
629 state (Figure supplement 6A). Stable reconstitution of *Tsc2*$^{-/-}$ MEFs with TSC2 also
630 decreased total glutathione levels (Figure 7B). To examine this response *in vivo*, we
631 employed a mouse model of tuberous sclerosis complex involving xenograft tumors
632 derived from the rat *TSC2*$^{-/-}$ tumor cell line ELT3 (Hodges et al., 2002). To avoid major
633 differences in tumor size from the treatments, we treated tumor-bearing mice for just 5

634 days with either vehicle or rapamycin, prior to harvesting tumors for immunoblot analysis
635 and metabolite profiling. Importantly, we found that rapamycin treatment strongly
636 decreased ATF4 protein levels in these tumors with a concomitant decrease in
637 glutathione levels, measured by LC-MS in tumor metabolite extracts (Figure 7C-D). An
638 analysis of published metabolomics data (Tang et al., 2019) also revealed that rapamycin
639 treatment significantly decreased glutathione levels in human TSC2-deficient
640 angiomyolipoma cells (Figure 7—figure supplement 6B). Likewise, inhibition of mTORC1
641 signaling with rapamycin or Torin1 in LNCaP and PC3 cells resulted in a significant
642 decrease in total glutathione levels, although the degree of decrease varied between the
643 two cell lines (Figure 7E), perhaps reflecting the above finding that SLC7A11 expression
644 is more resistant to mTOR inhibitors in PC3 cells (Figure supplement 5D-H).
645
646 To determine the role of ATF4 and SLC7A11-dependent cystine uptake in glutathione
647 synthesis downstream of mTORC1 signaling, we compared *Tsc2*$^{-/-}$ MEFs with or without
648 *Atf4* knockout. Total glutathione levels were greatly decreased in *Tsc2*$^{-/-}$ *Atf4*$^{-/-}$ MEFs, and
649 exogenous expression of ATF4 or SLC7A11, but not ATF4^{DBD}, was able to restore
650 glutathione levels to these cells (Figure 7F). Supplementation with all NEAAs or just
651 cysteine, transported through neutral amino acid systems, but not equimolar
652 concentrations of cystine, transported through SLC7A11, also rescued total glutathione
653 levels, as measured by either enzymatic assay or LC-MS (Figure 7F—figure supplement
654 6C). Furthermore, insulin stimulated an increase in glutathione levels in wild-type MEFs
655 in a manner completely sensitive to rapamycin, an effect ablated in *Atf4* knockout cells,
656 which had a very low abundance of glutathione (Figure 7G). Likewise, the rapamycin-
657 sensitive nature of glutathione in *Tsc2*$^{-/-}$ MEFs was completely lost in *Tsc2*$^{-/-}$ *Atf4*$^{-/-}$ MEFs
658 (Figure 7H). Glutathione levels were restored to these cells upon exogenous expression
659 of ATF4, but not the ATF4^{DBD} mutant. However, glutathione was still significantly reduced
660 with rapamycin treatment in cells expressing the rapamycin-resistant ATF4, suggesting
661 possible ATF4-independent mechanisms also contributing to this regulation (Lam et al.,
662 2017). As one possible contributing factor, we found that the transcripts encoding both
663 the catalytic (GCLC) and regulatory (GCLM) subunits of glutamate-cysteine ligase, the
664 first enzyme of glutathione synthesis, was sensitive rapamycin, in a manner unaffected

665 by ATF4 knockdown (Figure 7—figure supplement 6D-E). We also found that GCLC and
666 GCLM protein levels could be modestly induced by insulin through mTORC1 signaling in
667 both wild-type and ATF4 knockout cells, but their protein abundance was unaffected by
668 rapamycin in *Tsc2-/-* MEFs (Supplemental figure 6F-G). Thus, the mechanism underlying
669 the apparent ATF4-independent effects of mTORC1 signaling on glutathione levels
670 remain unknown. These collective data show that mTORC1 signaling induces glutathione
671 synthesis, at least in part, through the activation of ATF4 and SLC7A11-dependent
672 cystine uptake.
673
674 **Discussion**
675 Our findings expand the functional repertoire of mTORC1 signaling as it relates to the
676 control of anabolic processes and cellular metabolism through its noncanonical activation
677 of ATF4. Importantly, less than 10% of stress-responsive, ATF4-dependent targets were
678 found to be significantly stimulated through the mTORC1-mediated activation of ATF4 in
679 response to insulin. Among others, we found that genes involved in amino acid
680 biosynthesis, transport, and tRNA charging were induced by mTORC1-ATF4 signaling,
681 many to a comparable level to that of ER-stress induction with tunicamycin. While the
682 molecular nature of this selective induction remains unknown, our data suggest that the
683 61 ATF4-dependent genes shared in their induction between mTORC1 signaling and the
684 ISR represent targets most highly responsive to increases in ATF4 levels. Since mTORC1
685 signaling leads to a more modest increase in ATF4 protein levels than does the ISR, the
686 selective induction of these genes might be reminiscent of the dose-dependent activation
687 of MYC target genes documented in other studies (Sabò et al., 2014; Schuhmacher &
688 Eick, 2013; Walz et al., 2014). Our bioinformatic analyses and functional data also
689 indicate involvement of the C/EBP family of transcription factors as heterodimerization
690 partners of ATF4 for the regulation of these gene targets shared between mTORC1
691 signaling and the ISR.
692
693 Consistent with the specific ATF4 target genes induced by mTORC1 signaling, including
694 those involved in amino acid acquisition and tRNA charging, we found that ATF4
695 activation contributes to both canonical (e.g., protein synthesis) and new (e.g., glutathione

696 synthesis) functions of mTORC1. As mTORC1 stimulates protein synthesis through
697 multiple downstream targets (Holz et al., 2005; Jefferies et al., 1994; Ma & Blenis, 2009;
698 Raught et al., 2004; Thoreen et al., 2012), it was not surprising to find that ATF4 was
699 necessary but not sufficient for the increased rate of protein synthesis accompanying
700 mTORC1 activation. We also demonstrate that mTORC1 signaling regulates the
701 abundance of total cellular glutathione, both reduced and oxidized, at least in part through
702 the ATF4-dependent induction of the cystine transporter SLC7A11, a major source of the
703 cysteine that is limiting for glutathione synthesis. Importantly, this mTORC1-ATF4-
704 mediated transcriptional up-regulation of SLC7A11 leading to increased cystine uptake
705 would temporally follow the inhibition of SLC7A11 recently found to be mediated through
706 mTORC2 and Akt-dependent transient phosphorylation of the transporter (Gu et al., 2017;
707 Lien et al., 2017). Our findings are consistent with a recent study indicating rapamycin-
708 sensitive expression of xCT in TSC models, which the authors attribute to the OCT1
709 transcription factor (Li et al., 2019). However, our study indicates that the mTORC1-
710 mediated activation of ATF4 is both necessary and sufficient for this regulation. The
711 transcription factor NRF2 (also known as NFE2L2) is activated by oxidative stress and is
712 a master regulator of the enzymes required for glutathione synthesis, as well as SLC7A11
713 to increase cystine uptake (Habib et al., 2015; Sasaki et al., 2002; Ye et al., 2014). While
714 NRF2 depletion has been described to decrease the viability of cells with TSC gene loss
715 (Zarei et al., 2019), we have no evidence from this or previous studies that mTORC1
716 signaling influences the levels or activity of NRF2 (Zhang et al., 2014).
717
718 mTORC1 serves to couple growth signals to the coordinated control of anabolic
719 processes, including the biosynthesis of protein, lipids, and nucleotides, as well as
720 metabolic pathways that support this anabolic state (Valvezan & Manning, 2019). This
721 metabolic program is orchestrated to provide biosynthetic precursors and directly promote
722 the synthesis of macromolecules while also maintaining cellular homeostasis and
723 preventing nutrient or metabolic stress. For example, mTORC1 signaling promotes
724 metabolic flux through the NADPH-producing oxidative branch of the pentose phosphate
725 pathway, thereby providing the reducing power essential to support an mTORC1-
726 stimulated increase in *de novo* lipid synthesis (Duvel et al., 2010). Importantly, NADPH is

727 also essential to reduce cystine, taken up through SLC7A11, into two molecules of
728 cysteine for use in glutathione synthesis, in addition to being required to regenerate
729 reduced glutathione following its oxidation. Supporting this logic of a coordinated
730 metabolic program downstream of mTORC1, pro-growth signaling through mTORC1
731 likely promotes glutathione synthesis to help buffer against the oxidative stress that
732 accompanies anabolic metabolism and increased rates of protein synthesis (Han et al.,
733 2013; Harding et al., 2003; Kong & Chandel, 2018).
734
735 Our findings further support the addition of ATF4 to SREBP and HIF1, as nutrient- and
736 stress-sensing transcription factors that are independently co-opted by mTORC1
737 signaling to drive the expression of metabolic enzymes and nutrient transporters. Unlike
738 adaptive signals stemming from the depletion of individual nutrients, such as amino acids,
739 sterols, or oxygen, which generally attenuate mTORC1 signaling as part of the adaptive
740 response, pro-growth signals that activate mTORC1 can stimulate these transcription
741 factors in concert to support a broader anabolic program. It will be important in future
742 studies to understand the dual regulation of these transcription factors by both pro-growth
743 and adaptive mechanisms as it relates to settings of physiological (fasting and feeding)
744 and pathological (tumor development) nutrient fluctuations.
745
746 **Materials and Methods**
747

Key Resources Table				
Reagent type (species) or resource	**Designation**	**Source or reference**	**Identifiers**	**Additional information**
Biological sample (*M. musculus*)	ELT3 tumor samples	Valvezan et al., 2017	PMID:29056426	
cell line (*M. musculus*)	WT and *Tsc2*$^{-/-}$ MEFs	David Kwiatkowski	PMID:14561707	
cell line (*M. musculus*)	*eIF2*$\alpha^{A/A}$ MEFs	Randal Kaufman	PMID:11430820	

cell line (*M. musculus*)	*Rictor*$^{+/+}$ and *Rictor*$^{-/-}$ MEFs	D.A. Guertin and D.M. Sabatini	PMID:17141160	
cell line (*Homo-sapiens*)	PC3	ATCC	CRL-1435	
cell line (*Homo-sapiens*)	LNCaP	ATCC	CRL-1740	
cell line (*M. musculus*)	*Tsc2*$^{+/+}$ *Atf4*$^{-/-}$ MEFs	This paper		CRISPR-Cas9n generated – see methods
cell line (*M. musculus*)	*Tsc2*$^{-/-}$ *Atf4*$^{-/-}$ MEFs	This paper		CRISPR-Cas9n generated – see methods
transfected construct	Non-targeting pool	GE Life Sciences/Dharmacon	D-001810-10-50	
transfected construct (mouse)	Myc	GE Life Sciences/Dharmacon	L-040813-00-0010	
transfected construct (mouse)	Atf4	GE Life Sciences/Dharmacon	L-042737-01-0020	
transfected construct (mouse)	Rheb	GE Life Sciences/Dharmacon	L-057044-00-0020	
transfected construct (mouse)	RhebL1	GE Life Sciences/Dharmacon	L-056074-01-0020	
transfected construct (mouse)	Tsc2	GE Life Sciences/Dharmacon	L-047050-00-0020	
transfected construct (mouse)	C/ebpα	GE Life Sciences/Dharmacon	L-040561-00-0005	
transfected construct (mouse)	C/ebpβ	GE Life Sciences/Dharmacon	L-043110-00-0005	

transfected construct (mouse)	C/ebpδ	GE Life Sciences/Dharmacon	L-060294-01-0005	
transfected construct (mouse)	C/ebpγ	GE Life Sciences/Dharmacon	L-065627-00-0005	
transfected construct (human)	ATF4	GE Life Sciences/Dharmacon	L-005125-00-0020	
sequenced-based reagent	qPCR Primers	IDT		See table in methods
Recombinant DNA reagent	ATF4 (cDNA amplified from plasmid)	Addgene	Addgene 21845	
Recombinant DNA reagent	Pspax2 (Plasmid)	Addgene	Addgene 12260	
Recombinant DNA reagent	Pmd2.G (Plasmid)	Addgene	Addgene 12259	
Recombinant DNA reagent	pSpCas9n(BB)-2A-GFP (PX461) (Plasmid)	Addgene	Addgene 48140	
Recombinant DNA reagent	pTRIPZ (plasmid)	Alex Toker	PMID: 27088857	
Recombinant DNA reagent	GFP (cDNA amplified from plasmid)	Addgene	Addgene 19319	
Recombinant DNA reagent	SLC7A11 (cDNA amplified from plasmid)	Alex Toker	PMID: 29259101	
Recombinant DNA reagent	pBabe hygro IRES-TSC2	David Kwiatkowski	PMID: 15150095	
sequenced-based reagent	CRISPR-Cas9n guides for KO of ATF4	IDT		CACCGGAGGTGGAGGGGCTATGCT; AAACAGCA

				TAGCCCCT CCACCTCC; CACCGACA ATCTGCCTT CTCCAGG; AAACCCTG GAGAAGGC AGATTGTC
sequenced-based reagent	Sequencing Primers for Atf4$^{-/-}$ cell lines	IDT		TCGATGCT CTGTTTCGA ATG; CTTCTTCCC CCTTGCCTT AC
sequenced-based reagent	Primers for site-directed mutagenesis	IDT		GCCTCCTG CTCAGCCG CCGCCGCC TCGAGGTA CCCAGTGG CTGCTGTC TTGTTTTGC TCCATCT; AGATGGAG CAAAACAA GACAGCAG CCACTGGG TACCTCGA GGCGGCGG CGGCTGAG CAGGAGGC
Commercial assay or kit	KOD Xtreme™ Hot Start DNA Polymerase	Sigma Aldrich	71975	
antibody	(P)-S6K1 T389 Rabbit mAB	Cell Signaling Technologies (CST)	9234	1:1000
antibody	ATF4 Rabbit mAB	Cell Signaling Technologies (CST)	11815	1:1000
antibody	eIF2α Rabbit pAB	Cell Signaling Technologies	9722	1:1000
antibody	P-eIF2α S51 Rabbit pAB	Cell Signaling Technologies	9721	1:1000
antibody	S6K1 Rabbit mAB	Cell Signaling Technologies	2708	1:1000

antibody	CD98 Rabbit mAB	Cell Signaling Technologies	13180	1:1000
antibody	PSAT1 Rabbit pAB	Protein Tech	20180-1-AP	1:1000
antibody	MTHFD2 Rabbit pAB	Protein Tech	12270-1-AP	1:1000
antibody	AARS Rabbit pAB	Bethyl Antibodies	A303-475A-M	1:1000
antibody	GARS Rabbit pAB	Bethyl Antibodies	A304-746A-M	1:1000
antibody	LARS Rabbit pAB	Bethyl Antibodies	A304-316A-M	1:1000
antibody	XPOT Rabbit pAB	Aviva Biotechnologies	ARP40711_P050	1:1000
antibody	TSC2 Rabbit mAB	Cell Signaling Technologies	4308	1:1000
antibody	SLC7A11 (mouse) Rabbit mAB	Abcam	ab175186	1:1000
antibody	SLC7A11 (human) Rabbit mAB	Cell Signaling Technologies	12691	1:1000
antibody	GCLC Rabbit mAB	Abcam	ab190685	1:1000
antibody	GCLM Rabbit mAB	Abcam	ab126704	1:1000
antibody	β-actin Mouse mAB	Sigma	A5316	1:5000
chemical compound, drug	Doxycycline hydrochloride	Sigma	D3447	
chemical compound, drug	Rapamycin	LC Laboratories	R5000	
chemical compound, drug	Insulin	Alpha Diagnostic,	INSL 16-N-5	
chemical compound, drug	Tunicamycin	Sigma-Aldrich	T7765	

chemical compound, drug	Torin1	Tocris	4247	
chemical compound, drug	Erastin	Selleckchem	S7242	
chemical compound, drug	Buthionine-sulfoximine (BSO)	Sigma	B2515	
chemical compound, drug	Hygromycin B	Thermo Fisher Scientific	10687010	
chemical compound, drug	Puromycin	Sigma	P8833	
chemical compound, drug	Staurosporine	Tocris	1285	
chemical compound, drug	Cysteine	Sigma	C7477	
chemical compound, drug	Cystine	Sigma	57579	
chemical compound, drug	2-mercaptoethanol	EMD Millipore	444203	
chemical compound, drug	MEM Non-essential amino acids solution	Thermo Fisher Scientific	11140050	
chemical compound, drug	^{35}S-methionine	PerkinElmer	NEG009L005MC	
chemical compound, drug	L-[1, 2, 1', 2'-^{14}C]-Cystine	PerkinElmer	NEC854010UC	
Commercial assay or kit	FITC Annexin V Apoptosis Detection Kit I	BD	556547	
Commercial assay or kit	GSH/GSSG-Glo Assay	Promega	V6611	

748

749 **Cell culture**

750 MEFs and PC3 cells were maintained in Dulbecco's Modified Eagle's Medium (DMEM;
751 Corning/Cellgro, 10-017-CV) with 10% fetal bovine serum (FBS, Corning/Gibco). LNCaP

752 cells were maintained in RPMI-1640 (Corning/Cellgro 10-040-CV) with 10% FBS. *Tsc2*$^{-/-}$
753 (*p53*$^{-/-}$) MEFs and littermate derived wild-type counterparts were provided by David
754 Kwiatkowski (Brigham and Women's Hospital, Boston MA). *eIF2*$\alpha^{S/S}$ (WT) and *eIF2*$\alpha^{A/A}$
755 (S51A knock-in mutant) MEFs were provided by Randal Kaufman (Sanford-Burnham-
756 Prebys Medical Discovery Institute, La Jolla CA) and were not used above passage 3
757 (after received). *Rictor*$^{+/+}$ and *Rictor*$^{-/-}$ MEFs were provided by D.A. Guertin and D.M.
758 Sabatini (Whitehead Institute, Massachusetts Institute of Technology, Cambridge MA).
759 Cancer cell lines were obtained from ATCC. *Atf4*$^{-/-}$ MEF lines generated in this study were
760 maintained in DMEM with 10% FBS, supplemented with 55 μM 2-mercaptoethanol
761 (Thermo, 21985023) and 1X MEM nonessential amino acid mix (NEAA, final
762 concentrations: 100 μM each of alanine, aspartate, asparagine, glutamate, glycine,
763 proline, and serine; Thermo 11140050). In experiments with supplementation of excess
764 cysteine, cells were plated in DMEM with 10% FBS, 1 mM cysteine, and, where indicated,
765 1X MEM nonessential amino acid mix.
766
767 **siRNA knockdowns**
768 Cells were transfected with 20 nM of the indicated siRNAs using Opti-MEM (Thermo,
769 31985062) and RNAimax (Thermo, 13778150) according to the manufacturer's protocol.
770 siRNAs were from GE Life Sciences/Dharmacon: Non-targeting Pool (D-001810-10-50),
771 *Myc* (L-040813-00-0010), *Atf4* (mouse, L-042737-01-0020), *Rheb* (L-057044-00-0020),
772 *RhebL1* (L-056074-01-0020), *Tsc2* (L-047050-00-0020), C/ebpα (L-040561-00-0005),
773 C/ebpβ (L-043110-00-0005), C/ebpδ (L-060294-01-0005), C/ebpγ (L-065627-00-0005)
774 and *ATF4* (human, L-005125-00-0020). 48 h post-transfection, cells were treated as
775 indicated prior to lysis for immunoblotting, RNA extraction, or protein synthesis assays.
776 For C/EBP isoform knockdown experiments, transfection of siRNAs was performed a
777 second time, 24 h after the first transfection. For protein synthesis assays involving
778 siRNAs, transfection was also performed a second time, 24 h after the first transfection,
779 which was necessary to achieve sufficient knockdown of Rheb to reduce mTORC1
780 signaling.
781
782 **Generation and validation of *Atf4*$^{-/-}$ and reconstituted cell lines**

783 *Tsc2*$^{+/+}$ (WT) and *Tsc2*$^{-/-}$ MEFs lacking Atf4 were generated by CRISPR-Cas9 mediated
784 deletion using pSpCas9n(BB)-2A-GFP (PX461) vector (Addgene, 48140) according to
785 the previously described protocol (Ran et al., 2013). The paired nickase guides were
786 designed using E-CRISP (Heigwer et al., 2014) and targeted the sequences
787 AGCATAGCCCCTCCACCTCC and GACAATCTGCCTTCTCCAGG in Exon 2 of ATF4.
788 48 h post-transfection, single GFP-positive cells were sorted into 96-well plates. Cells
789 were cultured in DMEM with 10% FBS supplemented with 1X MEM NEAA and 55 μM 2-
790 mercaptoethanol. Single cell clones were grown for immunoblot analysis and those
791 showing loss of ATF4 protein were selected for sequence analysis involving the isolation
792 of genomic DNA (Qiagen, 69504), PCR amplification using KOD Xtreme™ Hot Start DNA
793 Polymerase (Millipore, 71975) and the primers TCGATGCTCTGTTTCGAATG and
794 CTTCTTCCCCCTTGCCTTAC flanking the targeted deletion site, with sequencing on an
795 ABI3730xl DNA analyzer at the DNA Resource Core of Dana-Farber/Harvard Cancer
796 Center (funded in part by NCI Cancer Center support grant 2P30CA006516-48). The
797 mutations were identified using CRISP-ID software (Dehairs et al., 2016). For the final
798 clones selected, the mutations generated in the WT MEFs include an out-of-frame 17-
799 base pair deletion starting at the codon encoding T237 and a large out-of-frame 73-base
800 pair deletion starting after the codon encoding G219, both resulting in premature STOP
801 codons. The mutations generated in the *Tsc2*$^{-/-}$ MEFs include an out-of-frame 245-base
802 pair deletion starting at the codon encoding G190, resulting in a premature STOP codon
803 after the D191 codon, and an in-frame deletion removing the sequences encoded
804 between E210 and E284.
805
806 For generation of *Atf4* expression vectors, the murine *Atf4* cDNA was amplified from the
807 plasmid 21845 from Addgene (Harding et al., 2000). Restriction enzyme cloning with AgeI
808 and ClaI was used to insert the *Atf4*-coding sequence (lacking the 5' and 3' UTR) into the
809 pTRIPZ plasmid for doxycycline-inducible expression. The ATF4^{DBD} mutant, in which
810 amino acids 292-298 of the DNA-binding domain are changed from RYRQKKR to
811 GYLEAAA (He et al., 2001; Lange et al., 2008) was generated by DpnI-mediated site-
812 directed mutagenesis using KOD Xtreme™ Hot Start DNA Polymerase. The dox-
813 inducible pTRIPZ and SLC7A11 plasmids were a gift from Alex Toker (Beth Israel

814 Deaconess Medical Center, Boston, MA). cDNA expression was induced with 1 μg/mL of
815 doxycycline (sigma-Aldrich, D3447) for 12-24 h before assays were conducted. GFP was
816 inserted into pTRIPZ to produce the control vector. Lentivirus was generated in HEK293T
817 cells transfected with pMD2.G and psPAX2 (Addgene, 12259 and 12260) and the given
818 pTRIPZ constructs. 48 h post-transfection, the virus-containing medium was used to
819 infect the *Atf4* knockout cells, which were selected with 8 μg/mL puromycin. TSC2
820 addback cell lines were generated by retroviral infection following transfection of PT67
821 cells with pBabe hygro IRES-EV or pBabe hygro IRES-TSC2. Cells were selected with
822 400 μg/mL hygromycin B (Thermo, 10687010).
823
824 **RNA-sequencing**
825 Wild-type and *Atf4*$^{-/-}$ MEFs were grown to 70% confluence in 6 cm plates and were serum-
826 starved in the presence of 2-mercaptoethanol and 1X MEM NEAA mixture and treated
827 with vehicle (DMSO) or 20 nM rapamycin (LC Laboratories, R5000) for 30 min prior to
828 stimulation with vehicle (water) or 500 nM insulin (Alpha Diagnostic, INSL 16-N-5) for 16
829 h or treated with vehicle (DMSO) or 2 μg/mL tunicamycin (Sigma-Aldrich, T7765) for 4,
830 8 or 16 h. RNA was harvested with TRIzol according to the manufacturer's protocol
831 (Thermo, 15596018). All samples passed RNA quality control measured by NanoDrop
832 1000 Spectrophotometer (NanoDrop Technologies) and 2100 Bioanalyzer (Agilent
833 Technologies). cDNA libraries were generated to produce 150 base pair paired-end reads
834 on an Illumina NovaSeq with read depth of 20 million paired reads per sample. Reads
835 were aligned and annotated to the Ensembl *Mus musculus* GRCm38.p6 genome
836 assembly using the align and featureCounts functions from the Rsubread package (2.0.1)
837 in R (3.6.3) (Liao et al., 2019). Differential gene expression analysis was performed using
838 the voom and eBayes functions from the EgdeR (3.28.1) and Limma (3.42.2) packages,
839 respectively (Ritchie et al., 2015; Robinson et al., 2009). Transcripts found to be
840 significantly induced by tunicamycin were further limited to those with a greater than 1.2-
841 fold increase. The enrichKEGG function from the clusterProfiler package (3.14.3) was
842 used to perform KEGG pathway over-representation tests (Yu et al., 2012). Gene set
843 enrichment analysis was evaluated using GSEA software from the Broad Institute
844 (Subramanian et al., 2005). Computations were run on the FASRC Cannon cluster,

845 supported by the Faculty of Arts and Sciences Division of Science Research Computing
846 Group at Harvard University. Pseudogenes and unannotated genes were excluded from
847 Figure 1C and supplementary Table 1. The source data can be found at GEO under the
848 accession number GSE158605.
849
850 **CiiiDER Analysis**
851 CiiiDER software was downloaded from CiiiDER.org with the *Mus musculus* GRCm38.94
852 genome files. Searches were run against the JASPAR transcription factor-binding profile
853 database. Searches were run on promoter regions spanning +1500 to -500 bp from the
854 predicted transcriptional start site using a site identification deficit threshold of 0.1. The
855 background gene list (ISR only) was comprised of the 200 ATF4-dependent genes most
856 significantly increased in expression upon tunicamycin treatment that were not in the list
857 of 61 genes shared in their regulation by mTORC1 signaling and the ISR. Results of this
858 analysis are included in supplemental table 2.
859
860 **Cistrome Analysis**
861 Each of the 61 shared mTORC1 and ISR genes were analyzed using the CistromeDB
862 Toolkit (http://dbtoolkit.cistrome.org/) of existing genome-wide ChIP-seq data. A half-
863 decay distance of 1 kb to the transcription start site was used. The top 20 transcription
864 factors or chromatin regulators found in ChIP-seq experiments to bind to each gene was
865 compiled, and the number of genes each factor bound to within the list of 61 was
866 determined, with the top 9 regulators graphed, excluding the general factors EP300 and
867 POL2RA.
868
869 **Immunoblotting**
870 Cells were lysed in ice-cold Triton lysis buffer (40mM HEPES pH 7.4, 120mM NaCl, 1mM
871 EDTA, 1% Triton X-100, 10mM sodium pyrophosphate, 10 mM glycerol 2-phosphate, 50
872 mM NaF, 0.5 mM sodium orthovanadate, 1 μM Microcystin-LR, and Sigma protease
873 inhibitor cocktail P8340). For immunoblots on SLC7A11, cells were lysed in 1% SDS lysis
874 buffer (10mM Tris pH 7.4, 1 mM EDTA, 10mM sodium pyrophosphate, 10 mM glycerol 2-
875 phosphate, 50 mM NaF, 0.5 mM sodium orthovanadate and Sigma protease inhibitor

876 cocktail P8340). Samples were centrifuged at 20,000 x g for 10 min at 4°C and protein
877 concentration in the supernatant was determined by Bradford assay (Bio-Rad, 5000202)
878 and normalized across samples. Proteins were separated by SDS-PAGE, transferred to
879 nitrocellulose membranes, and immunoblotted with indicated antibody. Primary
880 antibodies used: MTHFD2 (Protein Tech, 12270-1-AP), PSAT1 (Protein Tech 20180-1-
881 AP), phospho (P)-S6K1 T389 (Cell Signaling Technologies (CST), 9234), ATF4 (CST,
882 11815), eIF2α (CST, 9722), P-eIF2α S51 (CST, 9721), S6K1 (CST, 2708), CD98 (CST,
883 13180), AARS (Bethyl Antibodies, A303-475A-M), GARS (Bethyl Antibodies, A304-746A-
884 M) LARS (Bethyl Antibodies, A304-316A-M), XPOT (Aviva Biotechnologies,
885 ARP40711_P050), TSC2 (CST, 4308), SLC7A11 (mouse, Abcam, ab175186), SLC7A11
886 (human, CST, 12691), GCLC (Abcam, ab190685), GCLM (Abcam, ab126704), β-actin
887 (Sigma-Aldrich, A5316); secondary antibodies used: IRDye 800CW Donkey anti-Mouse
888 IgG (H + L) (LI-COR, 926-32212) and Donkey anti-Rabbit IgG (H + L) (LI-COR, 925-
889 32213), and HRP-conjugated anti-mouse and anti-rabbit secondary antibodies from
890 (CST, 7074 and 7076). Immunoblots of MTHFD2, PSAT1, AARS, GARS, LARS, and
891 XPOT were imaged using Odyssey CLx Imaging System (LI-COR Biosciences). β-actin
892 was developed with Odyssey CLx Imaging System or enhanced chemiluminescence
893 assay (ECL). All remaining immunoblots were developed using ECL. Immunoblots were
894 quantified using the Odyssey CLx Imaging System and were normalized to β-actin. he
895 ATF4 immunoblot corresponding to Figure 1B (graphed in supplemental Figure S1A) and
896 the SLC7A11 immunoblots in Figures 6D,E (graphed in supplemental Figures S5B,C)
897 were quantified using ImageJ and normalized to β-actin.
898
899 **NanoString analysis**
900 RNA was harvested using TRIzol from cells at 70% confluence. All samples passed RNA
901 quality control measured by NanoDrop 1000 Spectrophotometer. Parallel plates were
902 lysed for immunoblots. The isolated RNA was analyzed using a custom NanoString probe
903 library according to the manufacturer's instructions (NanoString Technologies). Briefly,
904 sample RNA was hybridized to RNA-probes at 65 °C for 16 h, excess probe was washed
905 away, and an nCounter SPRINT was used to quantify specific mRNA molecules present
906 in each sample. Direct mRNA counts were normalized to internal control genes and

907 mRNA expression was analyzed using nSOLVER software. Heatmaps were generated
908 with Morpheus software from the Broad Institute
909 (https://software.broadinstitute.org/morpheus). Transcripts with 100 counts or fewer, a
910 value based off of negative control samples, were not included in our analyses.
911
912 **qPCR**
913 For gene expression analysis, RNA was isolated with TRIzol according to the
914 manufacturer's protocol. All samples passed RNA quality control measured by NanoDrop
915 1000 Spectrophotometer. cDNA was generated with Superscript III First Strand Synthesis
916 System for RT-PCR (Thermo, 18080051). Quantitative RT-PCR was performed with a
917 CFX Connect Realtime PCR Detection System (Bio-Rad) using iTaq Universal SYBR
918 Green Supermix (Bio-Rad, 1725125). Samples were quantified by the ΔΔCT method,
919 normalized to *β-actin* (mouse samples) or *RPLP0* (human samples) to quantify relative
920 mRNA expression levels.
921
922 qPCR Primers:

Atf4	ATGGGTTCTCCAGCGACAAG	CCGGAAAAGGCATCCTCCTT
Psat1	GCTGTCGCCTTAGCACCA	TGGATCTCCAACAATACCGAGTG
Mthfd2	TCCTTGTTGTCTGCGTTGGC	CTTCATTTCGCACTGCCGCC
Slc7a5	GGACAAGGTGATGCGTCCAA	GCCAACACAATGTTCCCCAC
Aars	TTGCTATTCCCTCGGAGCAC	CTCCTCGGGAACCTTAGCTC
Gars	GGCAGAGGTCTCTGAGCTG	GCACGATGGTCATAAGCTGC
Cars	GAGCAGGCTGCCGACTACA	TATAGCTACGCGTGCTGAGG
Nars	GAGCCGGCCTGTGTAAAGAT	GACCCAGCCAAACACCTTCA
Iars	TATTGCATCACCTCCAGACGC	TGAACCATTCTGTTGCTGGGA
Gclc	TGTACTCCACCCTCGTCACCC	CTGCTGTCCCAAGGCTCG
Gclm	TGGGCACAGGTAAAACCCAA	CTGGGCTTCAATGTCAGGGA
Slc7a11	ATCTCCCCCAAGGGCATACT	GCATAGGACAGGGCTCCAAA
Slc3a2	TGATGAATGCACCCTTGTACTTG	GCTCCCCAGTGAAAGTGGA
Slc1a5	GTAAAATACCGCAATCCTGTATCC	CGATAGCGAAGACCACCAGG
c-Myc	AGAGCTCCTCGAGCTGTTTG	TTCTCTTCCTCGTCGCAGAT
C/ebpα	CAAGAACAGCAACGAGTACCG	GTCACTGGTCAACTCCAGCAC
C/ebpβ	CGCCTTATAAACCTCCCGCT	TGGCCACTTCCATGGGTCTA

C/ebpδ	CGACTTCAGCGCCTACATTGA	CTAGCGACAGACCCCACAC
C/ebpγ	TCGGATCACATTGCTCTGATTTC	TGTGCCTGAGTATGAATGACACT
Actin	CACTGTCGAGTCGCGTCC	TCATCCATGGCGAACTGGTG
PSAT1	AAAAACAATGGAGGTGCCGC	GGCTCCACTGGACAAACGTA
ASNS	TGGCTGCCTTTTATCAGGGG	TCTGCCACCTTTCTAGCAGC
MTHFD2	GGCAGTTCGAAATGAAGCTGTT	GCCAACCAGGATCACACTCA
SLC7A5	GACTACGCCTACATGCTGGA	AGCAGCAGCACGCAGAG
AARS	CCATTCAGAAGGGCACAGGT	TATCCACGCCCTGTGTTGTC
GARS	GCCAGCAGGGAGATCTTGTG	CCAGCTCCTTTGCTTCCAGA
XPOT	GACGCAGAGCGACTAGAGG	TAAACATCTTCCCTATCACTCCATC
SLC7A11	AAGGTGCCACTGTTCATCCC	ATGTTCTGGTTATTTTCTCCGACA
RPLP0	CCTCGTGGAAGTGACATCGT	ATCTGCTTGGAGCCCACATT

923

924 **Protein synthesis assay**

925 Cells were cultured as indicated, washed twice with PBS, and changed to
926 methionine/cystine/glutamine-free DMEM (Thermo, 21013024) supplemented with 0.5
927 mM L-cystine (Sigma, 57579) and L-glutamine (4 mM) with 50 μCi/mL ^{35}S-methionine
928 (PerkinElmer, NEG009L005MC) for 20 min. Cells were washed twice in ice cold PBS and
929 lysed in ice-cold Triton lysis buffer. Total protein concentrations were normalized following
930 a Bradford assay, and normalized samples were separated by SDS-PAGE and
931 transferred to nitrocellulose. ^{35}S-methionine incorporation into protein was analyzed by
932 autoradiography, and relative rates of protein synthesis were quantified using ImageJ
933 Software (NIH) to quantify radiolabeled protein per lane for each sample. For isogenic
934 *Atf4*$^{-/-}$ cell lines, exogenous cDNA expression was induced for 16 h with 150 ng/mL
935 doxycycline, and cells were treated as indicated in the presence of doxycycline (150
936 ng/mL) and 1X MEM NEAA mixture plus 1 mM cysteine (Sigma, C7477). Protein
937 synthesis was assayed with 20 min labeling in the absence of NEAA and cysteine to avoid
938 competition of ^{35}S-methionine uptake with the supplemented amino acids.

939

940 **Methionine and cystine uptake**

941 For methionine uptake assays, cells were cultured and labeled as described above for
942 the protein synthesis assay, were washed three times in cold PBS, and lysed in Triton
943 lysis buffer. For cystine uptake assays, cells were treated the same but labeled for the

944 final 10 min with medium containing 0.1 μCi L-[1, 2, 1', 2'-^{14}C]-Cystine (PerkinElmer,
945 NEC854010UC) and washed three times in ice-cold PBS containing cold cystine (1 mM),
946 prior to lysis in Triton lysis buffer. Whole-cell radiolabel incorporation was quantified with
947 a Beckman LS6500 scintillation counter. Cells from identically treated parallel plates were
948 counted using a Beckman Z1-Coulter Counter to normalize uptake measurements to cell
949 number.
950
951 **Proliferation assay**
952 To quantify cell proliferation, cells were plated in DMEM in 6-well plates in triplicate in the
953 presence of 2-mercaptoethanol, 1X MEM NEAA mixture, 10% FBS, and doxycycline (1
954 μg/mL). 24 h after plating, cells were washed twice with PBS and media was changed to
955 DMEM with 10% dialyzed FBS, doxycycline (1 μg/mL), and the amino acid supplements
956 indicated for each experiment, with media refreshed daily. Starting on day 0, viable cells
957 from triplicate wells corresponding to each condition or cell line were counted using a
958 hemocytometer, excluding dead cells detected by trypan blue stain (Sigma-Aldrich,
959 T8154).
960
961 **Analysis of cell death**
962 Cells were plated in DMEM in 6-well plates in triplicate in the presence of 2-
963 mercaptoethanol, MEM NEAA mixture, 10% FBS, and doxycycline (1 μg/mL). 24 h after
964 plating, cells were washed twice with PBS and media was changed to DMEM with 10%
965 dialyzed FBS and doxycycline (1 μg/mL). 72 h later, cells were detached with Accumax™
966 (Sigma-Aldrich, A7089) and washed twice with cold PBS on ice. Cells were stained with
967 Annexin V and propidium iodide (PI) according to manufacturer's instruction (BD,
968 556547). Samples were analyzed using an LSRFortessa (BD) flow cytometer, and the
969 fractions of stained cells were quantified using FloJo 10.6, with Staurosporine (4 h, 5 μM)
970 (Tocris, 1285) used as a positive control for cell death and to help establish gating of the
971 sorted cells.
972
973 **Measurements of cellular and tumor glutathione**

974 Cells were plated in 96-well plates at 5000 cells/well. Total glutathione, GSH, and GSSG
975 levels were measured using the GSH/GSSG-Glo Assay (Promega, V6611) according to
976 the manufacturer's protocol. Total glutathione levels were normalized to cell number
977 determined from parallel plates. BSO (Sigma, B2515) was used as a positive control to
978 inhibit glutathione synthesis.

979 For measurements via LC-MS/MS, metabolites were extracted from cells on dry ice using
980 80% methanol, and extracts were dried under nitrogen gas for metabolite profiling via
981 selected reaction monitoring (SRM) with polarity switching using a 5500 QTRAP mass
982 spectrometer. Data were analyzed using MultiQuant 2.1.1 software (AB/SCIEX) to
983 calculate the Q3 peak area. Normalized peak area of glutathione from human *TSC2*$^{-/-}$
984 angiomyolipoma (621-101) cells was determined from previously published data (Tang et
985 al., 2019). For xenograft tumor studies, experimental details were provided previously
986 (Valvezan et al., 2017). Briefly, mice bearing *TSC2*$^{-/-}$ ELT3 xenograft tumors were treated
987 every other day for 5 days with vehicle or rapamycin (1 mg/kg on day 1, 3, and 5) and
988 tumors were harvested for metabolite extraction, as above, 3 h after the final treatment.
989

990 **Statistics**

991 For RNA-sequencing analysis, Benjamini-Hochberg FDR-adjusted *P* values were
992 determined from empirical Bayes moderated t-statistics using the voom and eBayes
993 functions from the limma package. Comparisons with FDR-adjusted $P < 0.05$ were
994 considered significant for the gene groups denoted compared to vehicle-treated controls.
995 For KEGG enrichment, *P* values were false discovery rate corrected. For Ciiider
996 transcription factor over-representation analysis, Fisher's exact test *P* values were used.
997 Transcription factor binding elements with $P < 0.01$ and test statistic >0 were considered
998 over-represented in genes of interest. Unpaired two-tailed t-tests were used for
999 Nanostring analyses to calculate *P* values for rank ordering. All remaining statistical
1000 analysis was performed with Prism 8 software (GraphPad Software, La Jolla, California).
1001 Statistical analyses for qPCR data with two treatment groups were determined by
1002 unpaired two-tailed t-test, while those with greater than two treatment groups, were
1003 determined by one-way ANOVA with Holm-Sidak method for multiple comparisons.
1004 Statistical analyses for protein synthesis assays were determined by one-way ANOVA

1005 with Holm-Sidak method for multiple comparisons from values quantified with ImageJ
1006 software (US National Institutes of Health, Bethesda, Maryland). Statistical analyses for
1007 immunoblot quantification data with two treatment groups were determined by unpaired
1008 two-tailed t-test, while those with greater than two treatment groups, were determined by
1009 one-way ANOVA with Holm-Sidak method for multiple comparisons. For proliferation
1010 assays, unpaired two tailed t-test were used for comparisons to GFP-expressing cells.
1011 For cell death analysis, one-way ANOVA with Holm-Sidak method for multiple
1012 comparisons, summing the AnnexinV+/PI -, AnnexinV-/PI+, and AnnexinV+/PI+
1013 populations for each conditions. For glutathione quantification of experiments with two
1014 conditions, an unpaired two tailed t-test was performed. For remaining glutathione assays
1015 and all cystine and methionine uptake experiments, one-way ANOVA with Holm-Sidak
1016 method for multiple comparisons was used.
1017

1018 **Source Data**

1019 The source data for the RNA-sequencing experiment can be found at GEO under the
1020 accession number GSE158605.
1021

1022 **Acknowledgements**

1023 We thank David J. Kwiatkowski, Elizabeth P. Henske, Randal J. Kaufman, Alex Toker,
1024 and David M. Sabatini for cell lines and materials and Min Yuan, Gerta Hoxhaj, and Issam
1025 Ben-Sahra for technical assistance and critical discussions. This research was supported
1026 by grants from the NIH: T32-ES016645 (M.E.T.), F31-CA228332 (M.E.T.), R35-
1027 CA197459 (B.D.M.) and P01-CA120964 (B.D.M and J.A.); the Department of Defense's
1028 Congressionally Directed Medical Research Program on Tuberous Sclerosis Complex,
1029 award no. W81XWH-18-1-0659 (B.D.M.); and a research grant from Zafgen (B.D.M. and
1030 J.R.M.).
1031

1032 B.D.M. is a shareholder and scientific advisory board member of LAM Therapeutics and
1033 Navitor Pharmaceuticals. All other authors declare no competing financial interests.
1034

1035 **References**

1036

1037 Adams, C. M. (2007). Role of the transcription tactor ATF4 in the anabolic actions of
1038 insulin and the anti-anabolic actions of glucocorticoids. *J Biol Chem, 282*(23), 16744-
1039 16753. doi:10.1074/jbc.M610510200
1040 Arts, G.-J., Kuersten, S., Romby, P., Ehresmann, B., & Mattaj, I. W. (1998). The role of
1041 exportin-t in selective nuclear export of mature tRNAs. *EMBO J, 17*(24), 7430-7441.
1042 doi:10.1093/emboj/17.24.7430
1043 Bannai, S., & Kitamura, E. (1980). Transport interaction of L-cystine and L-glutamate in
1044 human diploid fibroblasts in culture. *J Biol Chem, 255*(6), 2372-2376.
1045 doi:10.1016/0026-0495(87)90207-1
1046 Ben-Sahra, I., Hoxhaj, G., Ricoult, S. J. H., Asara, J. M., & Manning, B. D. (2016).
1047 mTORC1 induces purine synthesis through control of the mitochondrial
1048 tetrahydrofolate cycle. *Science, 351*(6274), 728-733. doi:10.1126/science.aad0489
1049 Brugarolas, J., Lei, K., Hurley, R. L., Manning, B. D., Reiling, J. H., Hafen, E., Witters, L.
1050 A., Ellisen, L. W., & Kaelin, W. G., Jr. (2004). Regulation of mTOR function in
1051 response to hypoxia by REDD1 and the TSC1/TSC2 tumor suppressor complex.
1052 *Genes Dev, 18*(23), 2893-2904. doi:10.1101/gad.1256804
1053 Brugarolas, J. B., Vazquez, F., Reddy, A., Sellers, W. R., & Kaelin Jr, W. G. (2003).
1054 TSC2 regulates VEGF through mTOR-dependent and -independent pathways.
1055 *Cancer Cell, 4*(2), 147-158. doi:10.1016/S1535-6108(03)00187-9
1056 Clemens, M. J. (1996). Protein kinases that phosphorylate eIF2 and eIF2B, and their
1057 role in eukaryotic cell translational control. *Translational Control, 30*, 139-172.
1058 Cohen, D. M., Won, K.-J., Nguyen, N., Lazar, M. A., Chen, C. S., & Steger, D. J. (2015).
1059 ATF4 licenses C/EBPβ activity in human mesenchymal stem cells primed for
1060 adipogenesis. *eLife, 4*, e06821. doi:10.7554/eLife.06821
1061 Condon, K. J., Orozco, J. M., Adelmann, C. H., Spinelli, J. B., van der Helm, P. W.,
1062 Roberts, J. M., Kunchok, T., & Sabatini, D. M. (2021). Genome-wide CRISPR
1063 screens reveal multitiered mechanisms through which mTORC1 senses
1064 mitochondrial dysfunction. *Proc Natl Acad Sci U S A, 118*(4).
1065 doi:10.1073/pnas.2022120118

1066 Conrad, M., & Sato, H. (2012). The oxidative stress-inducible cystine/glutamate
1067 antiporter, system x c− : cystine supplier and beyond. *Amino Acids, 42*(1), 231-246.
1068 doi:10.1007/s00726-011-0867-5
1069 Csibi, A., Lee, G., Yoon, S.-O., Tong, H., Ilter, D., Elia, I., Fendt, S.-M., Roberts,
1070 Thomas M., & Blenis, J. (2014). The mTORC1/S6K1 pathway regulates glutamine
1071 metabolism through the eIF4B-dependent control of c-Myc translation. *Curr Biol,*
1072 *24*(19), 2274-2280. doi:10.1016/j.cub.2014.08.007
1073 Dehairs, J., Talebi, A., Cherifi, Y., & Swinnen, J. V. (2016). CRISP-ID: decoding
1074 CRISPR mediated indels by Sanger sequencing. *Sci Rep, 6*(1), 28973.
1075 doi:10.1038/srep28973
1076 Duvel, K., Yecies, J. L., Menon, S., Raman, P., Lipovsky, A. I., Souza, A. L.,
1077 Triantafellow, E., Ma, Q., Gorski, R., Cleaver, S., Vander Heiden, M. G., MacKeigan,
1078 J. P., Finan, P. M., Clish, C. B., Murphy, L. O., & Manning, B. D. (2010). Activation of
1079 a metabolic gene regulatory network downstream of mTOR complex 1. *Mol Cell, 39*.
1080 doi:10.1016/j.molcel.2010.06.022
1081 Ebert, S. M., Bullard, S. A., Basisty, N., Marcotte, G. R., Skopec, Z. P., Dierdorff, J. M.,
1082 Al-Zougbi, A., Tomcheck, K. C., DeLau, A. D., Rathmacher, J. A., Bodine, S. C.,
1083 Schilling, B., & Adams, C. M. (2020). Activating transcription factor 4 (ATF4)
1084 promotes skeletal muscle atrophy by forming a heterodimer with the transcriptional
1085 regulator C/EBPβ. *J Biol Chem, 295*(9), 2787-2803. doi:10.1074/jbc.RA119.012095
1086 Gearing, L. J., Cumming, H. E., Chapman, R., Finkel, A. M., Woodhouse, I. B., Luu, K.,
1087 Gould, J. A., Forster, S. C., & Hertzog, P. J. (2019). CiiiDER: A tool for predicting and
1088 analysing transcription factor binding sites. *PLOS ONE, 14*(9), e0215495.
1089 doi:10.1371/journal.pone.0215495
1090 Griffith, O. W., & Meister, A. (1979). Potent and specific inhibition of glutathione
1091 synthesis by buthionine sulfoximine (S-n-butyl homocysteine sulfoximine). *J Biol*
1092 *Chem, 254*(16), 7558-7560.
1093 Gu, Y., Albuquerque, C. P., Braas, D., Zhang, W., Villa, G. R., Bi, J., Ikegami, S., Masui,
1094 K., Gini, B., Yang, H., Gahman, T. C., Shiau, A. K., Cloughesy, T. F., Christofk, H. R.,
1095 Zhou, H., Guan, K. L., & Mischel, P. S. (2017). mTORC2 regulates amino acid

1096 metabolism in cancer by phosphorylation of the cystine-glutamate antiporter xCT. *Mol*
1097 *Cell, 67*(1), 128-138.e127. doi:10.1016/j.molcel.2017.05.030
1098 Habib, E., Linher-Melville, K., Lin, H. X., & Singh, G. (2015). Expression of xCT and
1099 activity of system xc(-) are regulated by NRF2 in human breast cancer cells in
1100 response to oxidative stress. *Redox Biol, 5*, 33-42. doi:10.1016/j.redox.2015.03.003
1101 Han, J., Back, S. H., Hur, J., Lin, Y.-H., Gildersleeve, R., Shan, J., Yuan, C. L.,
1102 Krokowski, D., Wang, S., Hatzoglou, M., Kilberg, M. S., Sartor, M. A., & Kaufman, R.
1103 J. (2013). ER-stress-induced transcriptional regulation increases protein synthesis
1104 leading to cell death. *Nat Cell Biol, 15*(5), 481-490. doi:10.1038/ncb2738
1105 Harding, H. P., Novoa, I., Zhang, Y., Zeng, H., Wek, R., Schapira, M., & Ron, D. (2000).
1106 Regulated translation initiation controls stress-induced gene expression in
1107 mammalian cells. *Mol Cell, 6*(5), 1099-1108. doi:10.1016/S1097-2765(00)00108-8
1108 Harding, H. P., Zhang, Y., Zeng, H., Novoa, I., Lu, P. D., Calfon, M., Sadri, N., Yun, C.,
1109 Popko, B., Paules, R., Stojdl, D. F., Bell, J. C., Hettmann, T., Leiden, J. M., & Ron, D.
1110 (2003). An integrated stress response regulates amino acid metabolism and
1111 resistance to oxidative stress. *Mol Cell, 11*(3), 619-633. doi:10.1016/S1097-
1112 2765(03)00105-9
1113 He, C. H., Gong, P., Hu, B., Stewart, D., Choi, M. E., Choi, A. M., & Alam, J. (2001).
1114 Identification of activating transcription factor 4 (ATF4) as an Nrf2-interacting protein.
1115 Implication for heme oxygenase-1 gene regulation. *J Biol Chem, 276*(24), 20858-
1116 20865. doi:10.1074/jbc.M101198200
1117 Heigwer, F., Kerr, G., & Boutros, M. (2014). E-CRISP: fast CRISPR target site
1118 identification. *Nat Methods, 11*(2), 122-123. doi:10.1038/nmeth.2812
1119 Hodges, L. C., Houston, K. D., Hunter, D. S., Fuchs-Young, R., Zhang, Z., Wineker, R.
1120 C., & Walker, C. L. (2002). Transdominant suppression of estrogen receptor signaling
1121 by progesterone receptor ligands in uterine leiomyoma cells. *Mol Cell Endocrinol,*
1122 *196*(1-2), 11-20. doi:10.1016/s0303-7207(02)00230-7
1123 Holz, M. K., Ballif, B. A., Gygi, S. P., & Blenis, J. (2005). mTOR and S6K1 mediate
1124 assembly of the translation preinitiation complex through dynamic protein interchange
1125 and ordered phosphorylation events. *Cell, 123*(4), 569-580.
1126 doi:10.1016/j.cell.2005.10.024

1127 Horton, J. D., Goldstein, J. L., & Brown, M. S. (2002). SREBPs: activators of the
1128 complete program of cholesterol and fatty acid synthesis in the liver. *J Clin Invest,*
1129 *109*(9), 1125-1131. doi:10.1172/JCI15593
1130 Hudson, C. C., Liu, M., Chiang, G. G., Otterness, D. M., Loomis, D. C., Kaper, F.,
1131 Giaccia, A. J., & Abraham, R. T. (2002). Regulation of hypoxia-inducible factor 1α
1132 expression and function by the mammalian target of rapamycin. *Mol Cell Biol, 22*(20),
1133 7004-7014. doi:10.1128/mcb.22.20.7004-7014.2002
1134 Huggins, C. J., Mayekar, M. K., Martin, N., Saylor, K. L., Gonit, M., Jailwala, P., Kasoji,
1135 M., Haines, D. C., Quiñones, O. A., & Johnson, P. F. (2015). C/EBPγ is a critical
1136 regulator of cellular stress response networks through heterodimerization with ATF4.
1137 *Mol Cell Biol, 36*(5), 693-713. doi:10.1128/mcb.00911-15
1138 Jefferies, H. B., Reinhard, C., Kozma, S. C., & Thomas, G. (1994). Rapamycin
1139 selectively represses translation of the "polypyrimidine tract" mRNA family. *PNAS,*
1140 *91*(10), 4441-4445. doi:10.1073/pnas.91.10.4441
1141 Kilberg, M. S., Shan, J., & Su, N. (2009). ATF4-dependent transcription mediates
1142 signaling of amino acid limitation. *Trends Endocrinol Metab, 20*(9), 436-443.
1143 doi:10.1016/j.tem.2009.05.008
1144 Kong, H., & Chandel, N. S. (2018). Regulation of redox balance in cancer and T cells. *J*
1145 *Biol Chem, 293*(20), 7499-7507. doi:10.1074/jbc.TM117.000257
1146 Kutay, U., Lipowsky, G., Izaurralde, E., Bischoff, F. R., Schwarzmaier, P., Hartmann, E.,
1147 & Görlich, D. (1998). Identification of a tRNA-Specific Nuclear Export Receptor. *Mol*
1148 *Cell, 1*(3), 359-369. doi:10.1016/S1097-2765(00)80036-2
1149 Lam, H. C., Baglini, C. V., Lope, A. L., Parkhitko, A. A., Liu, H.-J., Alesi, N., Malinowska,
1150 I. A., Ebrahimi-Fakhari, D., Saffari, A., Yu, J. J., Pereira, A., Khabibullin, D., Ogorek,
1151 B., Nijmeh, J., Kavanagh, T., Handen, A., Chan, S. Y., Asara, J. M., Oldham, W. M.,
1152 Diaz-Meco, M. T., Moscat, J., Sahin, M., Priolo, C., & Henske, E. P. (2017).
1153 p62/SQSTM1 cooperates with hyperactive mTORC1 to regulate glutathione
1154 production, maintain mitochondrial integrity, and promote tumorigenesis. *Cancer Res,*
1155 *77*(12), 3255. doi:10.1158/0008-5472.CAN-16-2458
1156 Lange, P. S., Chavez, J. C., Pinto, J. T., Coppola, G., Sun, C.-W., Townes, T. M.,
1157 Geschwind, D. H., & Ratan, R. R. (2008). ATF4 is an oxidative stress-inducible,

1158 prodeath transcription factor in neurons in vitro and in vivo. *J Exp Med, 205*(5), 1227-
1159 1242. doi:10.1084/jem.20071460
1160 Laughner, E., Taghavi, P., Chiles, K., Mahon, P. C., & Semenza, G. L. (2001). HER2
1161 (neu) signaling increases the rate of hypoxia-inducible factor 1α (HIF-1α) synthesis:
1162 novel mechanism for HIF-1-mediated vascular endothelial growth factor expression.
1163 *Mol Cell Biol, 21*(12), 3995-4004. doi:10.1128/mcb.21.12.3995-4004.2001
1164 Lee, J. H., Budanov, A. V., Park, E. J., Birse, R., Kim, T. E., Perkins, G. A., Ocorr, K.,
1165 Ellisman, M. H., Bodmer, R., Bier, E., & Karin, M. (2010). Sestrin as a feedback
1166 inhibitor of TOR that prevents age-related pathologies. *Science, 327*(5970), 1223-
1167 1228. doi:10.1126/science.1182228
1168 Li, C., Chen, H., Lan, Z., He, S., Chen, R., Wang, F., Liu, Z., Li, K., Cheng, L., Liu, Y.,
1169 Sun, K., Wan, X., Chen, X., Peng, H., Li, L., Zhang, Y., Jing, Y., Huang, M., Wang,
1170 Y., Wang, Y., Jiang, J., Zha, X., Chen, L., & Zhang, H. (2019). mTOR-dependent
1171 upregulation of xCT blocks melanin synthesis and promotes tumorigenesis. *Cell*
1172 *Death & Diff, 26*(10), 2015-2028. doi:10.1038/s41418-019-0274-0
1173 Liao, Y., Smyth, G. K., & Shi, W. (2019). The R package Rsubread is easier, faster,
1174 cheaper and better for alignment and quantification of RNA sequencing reads.
1175 *Nucleic Acids Res, 47*(8), e47. doi:10.1093/nar/gkz114
1176 Lien, E. C., Ghisolfi, L., Geck, R. C., Asara, J. M., & Toker, A. (2017). Oncogenic PI3K
1177 promotes methionine dependency in breast cancer cells through the cystine-
1178 glutamate antiporter xCT. *Sci Sig, 10*(510), eaao6604. doi:10.1126/scisignal.aao6604
1179 Ma, X. M., & Blenis, J. (2009). Molecular mechanisms of mTOR-mediated translational
1180 control. *Nat Rev Mol Cell Biol, 10*(5), 307-318. doi:10.1038/nrm2672
1181 Mei, S., Qin, Q., Wu, Q., Sun, H., Zheng, R., Zang, C., Zhu, M., Wu, J., Shi, X., Taing,
1182 L., Liu, T., Brown, M., Meyer, C. A., & Liu, X. S. (2017). Cistrome Data Browser: a
1183 data portal for ChIP-Seq and chromatin accessibility data in human and mouse.
1184 *Nucleic Acids Res, 45*(D1), D658-d662. doi:10.1093/nar/gkw983
1185 Meister, A. (1983). Selective modification of glutathione metabolism. *Science,*
1186 *220*(4596), 472-477. doi:10.1126/science.6836290
1187 Nakazawa, M. S., Keith, B., & Simon, M. C. (2016). Oxygen availability and metabolic
1188 adaptations. *Nat Rev Cancer, 16*(10), 663-673. doi:10.1038/nrc.2016.84

1189 Newman, J. R. S., & Keating, A. E. (2003). Comprehensive identification of human bZIP
1190 interactions with coiled-coil arrays. *Science, 300*(5628), 2097.
1191 doi:10.1126/science.1084648
1192 Owen, J. L., Zhang, Y., Bae, S.-H., Farooqi, M. S., Liang, G., Hammer, R. E., Goldstein,
1193 J. L., & Brown, M. S. (2012). Insulin stimulation of SREBP-1c processing in
1194 transgenic rat hepatocytes requires p70 S6-kinase. *PNAS, 109*(40), 16184.
1195 doi:10.1073/pnas.1213343109
1196 Ozcan, U., Ozcan, L., Yilmaz, E., Düvel, K., Sahin, M., Manning, B. D., & Hotamisligil,
1197 G. S. (2008). Loss of the tuberous sclerosis complex tumor suppressors triggers the
1198 Unfolded protein response to regulate insulin signaling and apoptosis. *Mol Cell,*
1199 *29*(5), 541-551. doi:10.1016/j.molcel.2007.12.023
1200 Park, Y., Reyna-Neyra, A., Philippe, L., & Thoreen, C. C. (2017). mTORC1 balances
1201 cellular amino acid supply with demand for protein synthesis through post-
1202 transcriptional control of ATF4. *Cell Rep, 19*(6), 1083-1090.
1203 doi:10.1016/j.celrep.2017.04.042
1204 Peterson, Timothy R., Sengupta, Shomit S., Harris, Thurl E., Carmack, Anne E., Kang,
1205 Seong A., Balderas, E., Guertin, David A., Madden, Katherine L., Carpenter, Anne E.,
1206 Finck, Brian N., & Sabatini, David M. (2011). mTOR complex 1 regulates lipin 1
1207 localization to control the SREBP pathway. *Cell, 146*(3), 408-420.
1208 doi:10.1016/j.cell.2011.06.034
1209 Porstmann, T., Santos, C. R., Griffiths, B., Cully, M., Wu, M., Leevers, S., Griffiths, J. R.,
1210 Chung, Y.-L., & Schulze, A. (2008). SREBP activity is regulated by mTORC1 and
1211 contributes to Akt-dependent cell growth. *Cell Metab, 8*(3), 224-236.
1212 doi:10.1016/j.cmet.2008.07.007
1213 Ran, F. A., Hsu, P. D., Wright, J., Agarwala, V., Scott, D. A., & Zhang, F. (2013).
1214 Genome engineering using the CRISPR-Cas9 system. *Nat Protoc, 8*(11), 2281-2308.
1215 doi:10.1038/nprot.2013.143
1216 Raught, B., Peiretti, F., Gingras, A. C., Livingstone, M., Shahbazian, D., Mayeur, G. L.,
1217 Polakiewicz, R. D., Sonenberg, N., & Hershey, J. W. (2004). Phosphorylation of
1218 eucaryotic translation initiation factor 4B Ser422 is modulated by S6 kinases. *EMBO*
1219 *J, 23*(8), 1761-1769. doi:10.1038/sj.emboj.7600193

1220 Reiling, J. H., & Hafen, E. (2004). The hypoxia-induced paralogs Scylla and Charybdis
1221 inhibit growth by down-regulating S6K activity upstream of TSC in Drosophila. *Genes*
1222 *Dev, 18*(23), 2879-2892. doi:10.1101/gad.322704
1223 Ritchie, M. E., Phipson, B., Wu, D., Hu, Y., Law, C. W., Shi, W., & Smyth, G. K. (2015).
1224 limma powers differential expression analyses for RNA-sequencing and microarray
1225 studies. *Nucleic Acids Res, 43*(7), e47. doi:10.1093/nar/gkv007
1226 Robinson, M. D., McCarthy, D. J., & Smyth, G. K. (2009). edgeR: a Bioconductor
1227 package for differential expression analysis of digital gene expression data.
1228 *Bioinformatics, 26*(1), 139-140. doi:10.1093/bioinformatics/btp616
1229 Sabò, A., Kress, T. R., Pelizzola, M., de Pretis, S., Gorski, M. M., Tesi, A., Morelli, M. J.,
1230 Bora, P., Doni, M., Verrecchia, A., Tonelli, C., Fagà, G., Bianchi, V., Ronchi, A., Low,
1231 D., Müller, H., Guccione, E., Campaner, S., & Amati, B. (2014). Selective
1232 transcriptional regulation by Myc in cellular growth control and lymphomagenesis.
1233 *Nature, 511*(7510), 488-492. doi:10.1038/nature13537
1234 Sasaki, H., Sato, H., Kuriyama-Matsumura, K., Sato, K., Maebara, K., Wang, H.,
1235 Tamba, M., Itoh, K., Yamamoto, M., & Bannai, S. (2002). Electrophile response
1236 element-mediated induction of the cystine/glutamate exchange transporter gene
1237 expression. *J Biol Chem, 277*(47), 44765-44771. doi:10.1074/jbc.M208704200
1238 Scheuner, D., Song, B., McEwen, E., Liu, C., Laybutt, R., Gillespie, P., Saunders, T.,
1239 Bonner-Weir, S., & Kaufman, R. J. (2001). Translational control is required for the
1240 unfolded protein response and in vivo glucose homeostasis. *Mol Cell, 7*(6), 1165-
1241 1176. doi:10.1016/S1097-2765(01)00265-9
1242 Schuhmacher, M., & Eick, D. (2013). Dose-dependent regulation of target gene
1243 expression and cell proliferation by c-Myc levels. *Transcription, 4*(4), 192-197.
1244 doi:10.4161/trns.25907
1245 Stine, Z. E., Walton, Z. E., Altman, B. J., Hsieh, A. L., & Dang, C. V. (2015). MYC,
1246 metabolism, and cancer. *Cancer Discovery, 5*(10), 1024. doi:10.1158/2159-8290.CD-
1247 15-0507
1248 Subramanian, A., Tamayo, P., Mootha, V. K., Mukherjee, S., Ebert, B. L., Gillette, M. A.,
1249 Paulovich, A., Pomeroy, S. L., Golub, T. R., Lander, E. S., & Mesirov, J. P. (2005).
1250 Gene set enrichment analysis: A knowledge-based approach for interpreting

1251 genome-wide expression profiles. *PNAS, 102*(43), 15545.
1252 doi:10.1073/pnas.0506580102
1253 Tang, Y., El-Chemaly, S., Taveira-Dasilva, A., Goldberg, H. J., Bagwe, S., Rosas, I. O.,
1254 Moss, J., Priolo, C., & Henske, E. P. (2019). Alterations in Polyamine Metabolism in
1255 Patients With Lymphangioleiomyomatosis and Tuberous Sclerosis Complex 2-
1256 Deficient Cells. *Chest, 156*(6), 1137-1148. doi: 10.1016/j.chest.2019.05.038
1257 Thomas, G. V., Tran, C., Mellinghoff, I. K., Welsbie, D. S., Chan, E., Fueger, B.,
1258 Czernin, J., & Sawyers, C. L. (2006). Hypoxia-inducible factor determines sensitivity
1259 to inhibitors of mTOR in kidney cancer. *Nat Med, 12*(1), 122-127.
1260 doi:10.1038/nm1337
1261 Thoreen, C. C., Chantranupong, L., Keys, H. R., Wang, T., Gray, N. S., & Sabatini, D.
1262 M. (2012). A unifying model for mTORC1-mediated regulation of mRNA translation.
1263 *Nature, 485*(7396), 109-113. doi:10.1038/nature11083
1264 Torrence, M. E., & Manning, B. D. (2018). Nutrient Sensing in Cancer. *Ann Rev of*
1265 *Cancer Biol, 2*(1), 251-269. doi:10.1146/annurev-cancerbio-030617-050329
1266 Valvezan, A. J., & Manning, B. D. (2019). Molecular logic of mTORC1 signalling as a
1267 metabolic rheostat. *Nat Metab, 1*(3), 321-333. doi:10.1038/s42255-019-0038-7
1268 Valvezan, A. J., Turner, M., Belaid, A., Lam, H. C., Miller, S. K., McNamara, M. C.,
1269 Baglini, C., Housden, B. E., Perrimon, N., Kwiatkowski, D. J., Asara, J. M., Henske,
1270 E. P., & Manning, B. D. (2017). mTORC1 couples nucleotide synthesis to nucleotide
1271 demand resulting in a targetable metabolic vulnerability. *Cancer Cell, 32*(5), 624-
1272 638.e625. doi:10.1016/j.ccell.2017.09.013
1273 Vattem, K. M., & Wek, R. C. (2004). Reinitiation involving upstream ORFs regulates
1274 ATF4 mRNA translation in mammalian cells. *PNAS, 101*(31), 11269-11274.
1275 doi:10.1073/pnas.0400541101
1276 Wall, M., Poortinga, G., Hannan, K. M., Pearson, R. B., Hannan, R. D., & McArthur, G.
1277 A. (2008). Translational control of c-MYC by rapamycin promotes terminal myeloid
1278 differentiation. *Blood, 112*(6), 2305-2317. doi:10.1182/blood-2007-09-111856
1279 Walter, P., & Ron, D. (2011). The unfolded protein response: from stress pathway to
1280 homeostatic regulation. *Science, 334*(6059), 1081. doi:10.1126/science.1209038

1281 Walz, S., Lorenzin, F., Morton, J., Wiese, K. E., von Eyss, B., Herold, S., Rycak, L.,
1282 Dumay-Odelot, H., Karim, S., Bartkuhn, M., Roels, F., Wüstefeld, T., Fischer, M.,
1283 Teichmann, M., Zender, L., Wei, C.-L., Sansom, O., Wolf, E., & Eilers, M. (2014).
1284 Activation and repression by oncogenic MYC shape tumour-specific gene expression
1285 profiles. *Nature, 511*(7510), 483-487. doi:10.1038/nature13473
1286 Wolfson, R. L., Chantranupong, L., Saxton, R. A., Shen, K., Scaria, S. M., Cantor, J. R.,
1287 & Sabatini, D. M. (2016). Sestrin2 is a leucine sensor for the mTORC1 pathway.
1288 *Science, 351*(6268), 43-48. doi:10.1126/science.aab2674
1289 Wortel, I. M. N., van der Meer, L. T., Kilberg, M. S., & van Leeuwen, F. N. (2017).
1290 Surviving stress: modulation of ATF4-mediated stress responses in normal and
1291 malignant cells. *Trends in endocrinology and metabolism: TEM, 28*(11), 794-806.
1292 doi:10.1016/j.tem.2017.07.003
1293 Wu, H., Wei, L., Fan, F., Ji, S., Zhang, S., Geng, J., Hong, L., Fan, X., Chen, Q., Tian,
1294 J., Jiang, M., Sun, X., Jin, C., Yin, Z.-Y., Liu, Q., Zhang, J., Qin, F., Lin, K.-H., Yu, J.-
1295 S., Deng, X., Wang, H.-R., Zhao, B., Johnson, R. L., Chen, L., & Zhou, D. (2015).
1296 Integration of Hippo signalling and the unfolded protein response to restrain liver
1297 overgrowth and tumorigenesis. *Nature Communications, 6*(1), 6239.
1298 doi:10.1038/ncomms7239
1299 Xiao, Y., Hill, M. C., Li, L., Deshmukh, V., Martin, T. J., Wang, J., & Martin, J. F. (2019).
1300 Hippo pathway deletion in adult resting cardiac fibroblasts initiates a cell state
1301 transition with spontaneous and self-sustaining fibrosis. *Genes Dev, 33*(21-22), 1491-
1302 1505. doi:10.1101/gad.329763.119
1303 Yang, W. S., & Stockwell, B. R. (2008). Synthetic lethal screening identifies compounds
1304 activating iron-dependent, nonapoptotic cell death in oncogenic-RAS-harboring
1305 cancer cells. *Chem Biol, 15*(3), 234-245. doi:10.1016/j.chembiol.2008.02.010
1306 Ye, P., Mimura, J., Okada, T., Sato, H., Liu, T., Maruyama, A., Ohyama, C., & Itoh, K.
1307 (2014). Nrf2- and ATF4-Dependent Upregulation of xCT Modulates the Sensitivity of
1308 T24 Bladder Carcinoma Cells to Proteasome Inhibition. *Mol Cell Biol, 34*(18), 3421.
1309 doi:10.1128/MCB.00221-14

1310 Yu, G., Wang, L. G., Han, Y., & He, Q. Y. (2012). clusterProfiler: an R package for
1311 comparing biological themes among gene clusters. *Omics, 16*(5), 284-287.
1312 doi:10.1089/omi.2011.0118
1313 Zarei, M., Du, H., Nassar, A. H., Yan, R. E., Giannikou, K., Johnson, S. H., Lam, H. C.,
1314 Henske, E. P., Wang, Y., Zhang, T., Asara, J., & Kwiatkowski, D. J. (2019). Tumors
1315 with TSC mutations are sensitive to CDK7 inhibition through NRF2 and glutathione
1316 depletion. *J Exp Med, 216*(11), 2635-2652. doi:10.1084/jem.20190251
1317 Zhang, Y., Nicholatos, J., Dreier, J. R., Ricoult, S. J. H., Widenmaier, S. B., Hotamisligil,
1318 G. S., Kwiatkowski, D. J., & Manning, B. D. (2014). Coordinated regulation of protein
1319 synthesis and degradation by mTORC1. *Nature, 513*(7518), 440-443.
1320 doi:10.1038/nature13492
1321 Zheng, R., Wan, C., Mei, S., Qin, Q., Wu, Q., Sun, H., Chen, C.-H., Brown, M., Zhang,
1322 X., Meyer, C. A., & Liu, X S. (2019). Cistrome Data Browser: expanded datasets and
1323 new tools for gene regulatory analysis. *Nucleic Acids Res, 47*(D1), D729-D735.
1324 doi:10.1093/nar/gky1094
1325 Zhong, H., Chiles, K., Feldser, D., Laughner, E., Hanrahan, C., Georgescu, M. M.,
1326 Simons, J. W., & Semenza, G. L. (2000). Modulation of hypoxia-inducible factor
1327 1alpha expression by the epidermal growth factor/phosphatidylinositol 3-
1328 kinase/PTEN/AKT/FRAP pathway in human prostate cancer cells: implications for
1329 tumor angiogenesis and therapeutics. *Cancer Res, 60*(6), 1541-1545.
1330 Zirin, J., Ni, X., Sack, L. M., Yang-Zhou, D., Hu, Y., Brathwaite, R., Bulyk, M. L.,
1331 Elledge, S. J., & Perrimon, N. (2019). Interspecies analysis of MYC targets identifies
1332 tRNA synthetases as mediators of growth and survival in MYC-overexpressing cells.
1333 *PNAS, 116*(29), 14614. doi:10.1073/pnas.1821863116
1334

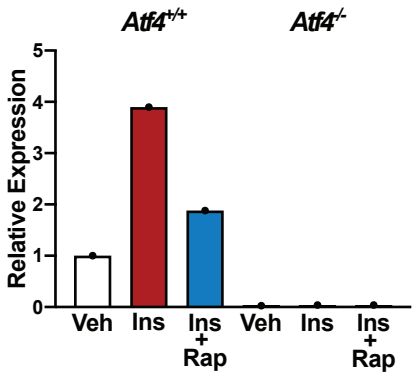

Supplemental Figure 1. Data related to Figure 1.
(A) Quantification of immunoblot shown in Figure 1B.

Figure 3—figure supplement 2

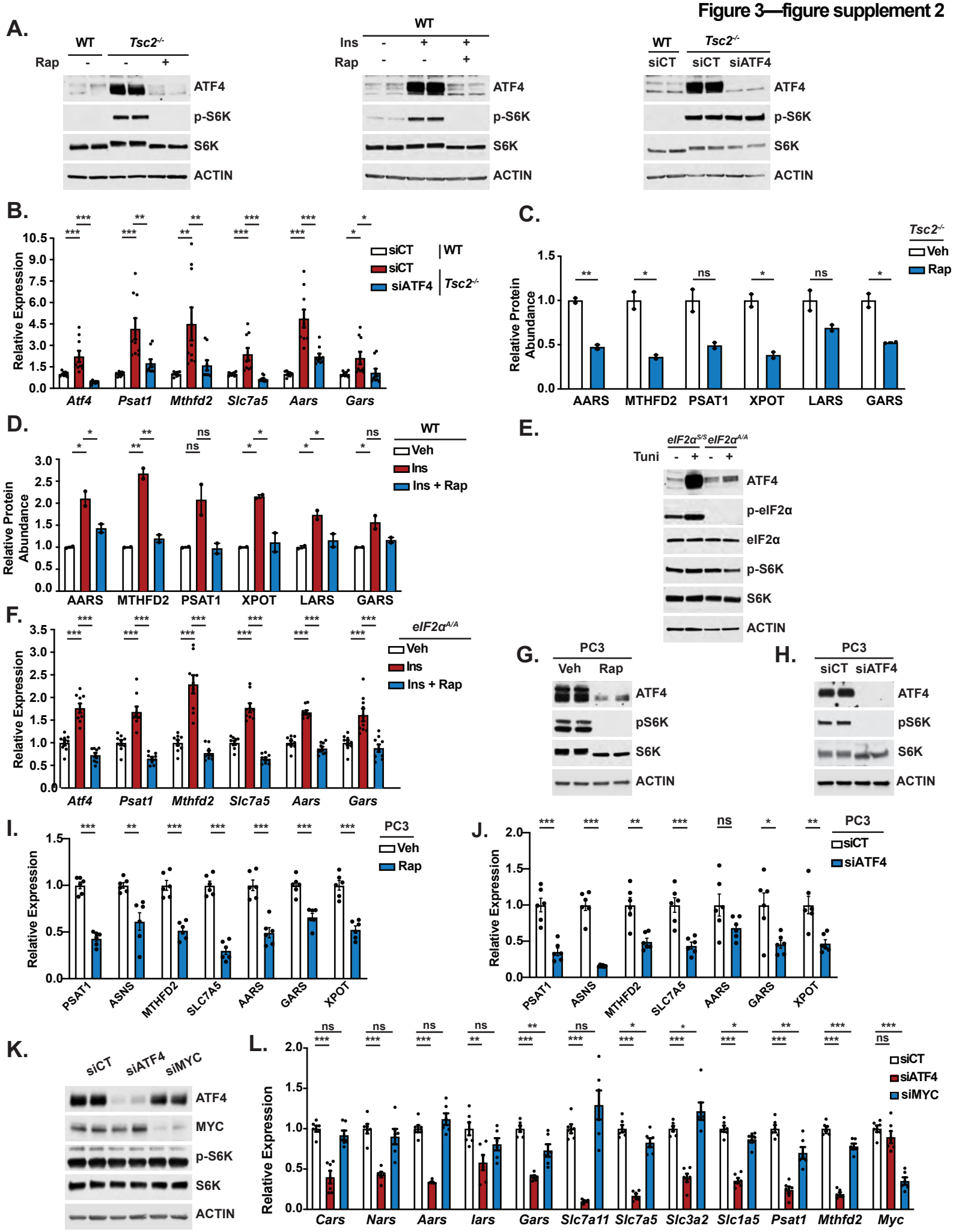

1337 **Supplemental Figure 2. Data related to Figure 3**.
1338 (A) Representative immunoblots corresponding to Nanostring heatmaps depicted in
1339 Figure 2A, with biological duplicates shown.
1340 (B) qPCR analysis of the indicated transcripts in *Tsc2*$^{-/-}$ MEFs transfected with siRNAs as
1341 described in Figure 3A. Expression relative to non-targeting control (siCT) is graphed as
1342 mean ± SEM from three independent experiments, each with 3 biological replicates (n=9).
1343 (C, D) Quantification of immunoblots shown in Figure 2D,E.
1344 (E) Representative immunoblot of *eIF2*$\alpha^{A/A}$ MEFs treated with vehicle or tunicamycin (2
1345 µg/mL, 4 h).
1346 (F) qPCR analysis of the indicated transcripts in eIF2$\alpha^{A/A}$ MEFs treated as described in
1347 Figure 2F. Expression relative to vehicle-treated, unstimulated cells is graphed as mean
1348 ± SEM from three independent experiments, each with 3 biological replicates (n=9).
1349 (G,H) Representative immunoblots of serum-deprived PC3 cells treated with vehicle or
1350 rapamycin (20 nM, 16 h) (G) or transfected with *Atf4* siRNAs or non-targeting controls
1351 (siCT) prior to serum-deprivation (16h) (H), with biological duplicates for each condition
1352 shown.
1353 (I,J) qPCR analysis of the indicated transcripts in cells treated as described in (G,H).
1354 (K) Representative immunoblots of *Tsc2*$^{-/-}$ MEFs transfected with control siRNAs (siCT)
1355 or those targeting *Atf4* or *c-Myc* prior to 16 h serum-deprivation.
1356 (L) qPCR analysis of the indicated transcripts in cells transfected as described in (K).
1357 Expression relative to siCT transfected cells is graphed as mean ± SEM from two
1358 independent experiments, each with 3 biological replicates (n=6).
1359 (A,E,G,H,K) are representative of at least two independent experiments. *$p < 0.05$, **$p <$
1360 0.01, ***$p < 0.001$, ns = not significant, calculated in (B,D,F, L) via one-way ANOVA with
1361 Holm-Sidak method for multiple comparisons and (C,I,J) via unpaired two tailed t-test.

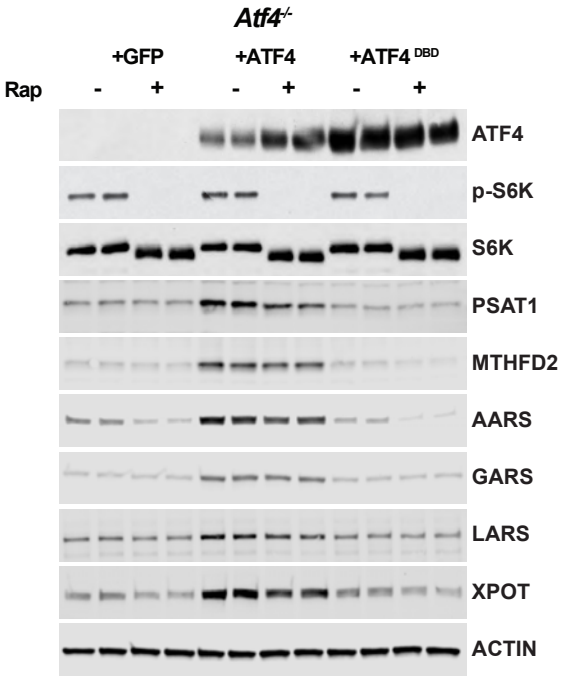

Supplemental Figure 3. Data related to Figure 4.
(A) Representative immunoblots of serum-deprived *Tsc2*$^{-/-}$ MEFs (*Atf4* WT) and *Tsc2*$^{-/-}$ *Atf4*$^{-/-}$ MEFs with stable expression of cDNAs encoding GFP, ATF4 lacking its 5'UTR, or a DNABD mutant (DBD) of this ATF4 treated with vehicle or rapamycin (20 nM, 16 h), with biological duplicates for each condition shown.

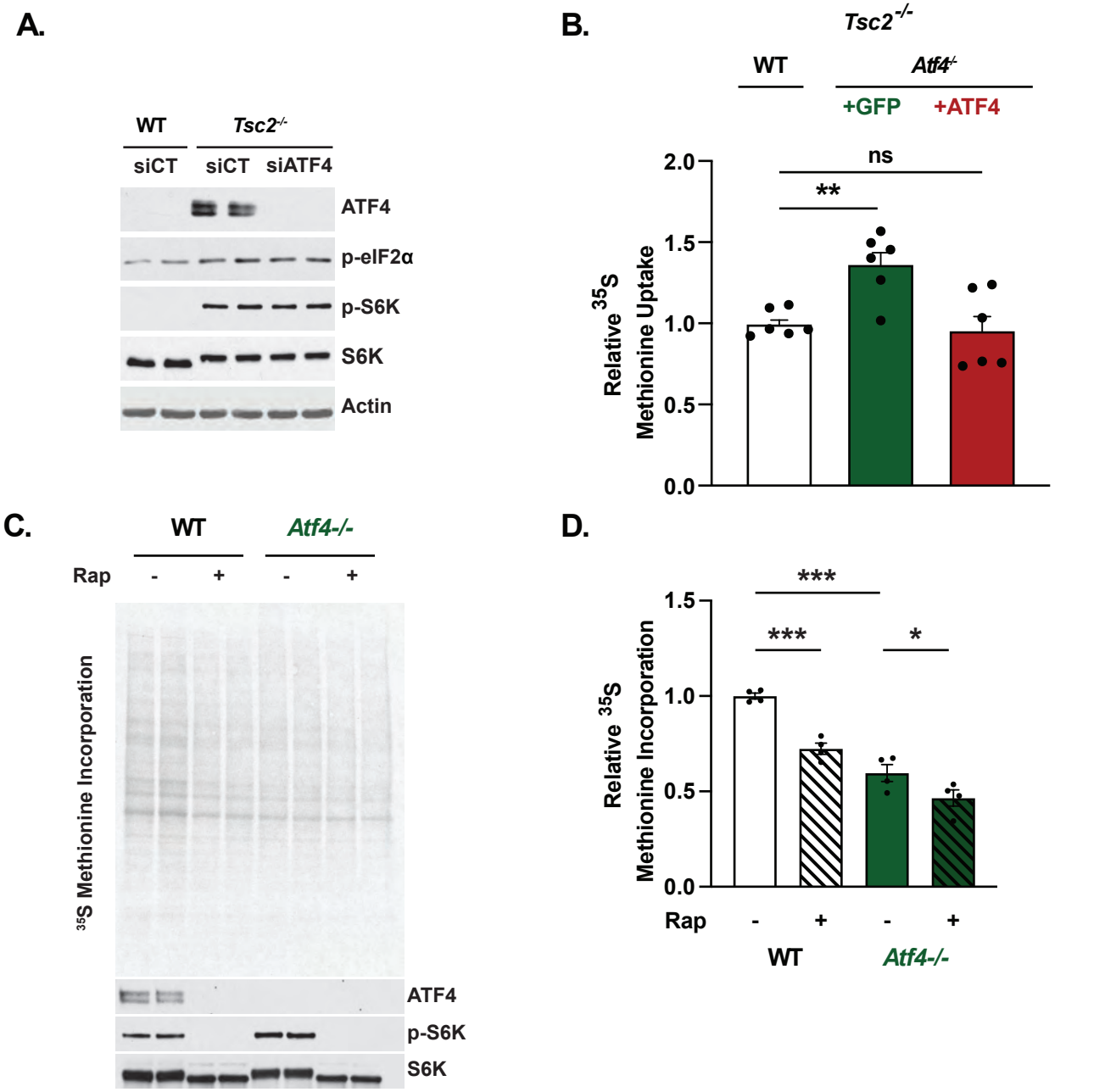

Supplemental Figure 4. Data related to Figure 5.
(A) Representative immunoblots of *Tsc2*$^{-/-}$ MEFs transfected with *Atf4, Rheb*, or non-targeting control (siCT) siRNAs prior to serum starvation for 16h, with biological duplicates shown. Data is representative of at least three independent experiments.
(B) Cellular methionine uptake in serum-deprived *Tsc2*$^{-/-}$ MEFs (*Atf4* WT) and *Tsc2*$^{-/-}$ *Atf4*$^{-/-}$ MEFs with stable expression of cDNAs encoding GFP or ATF4 was assayed and graphed as mean ± SEM relative to WT cells with data from two independent experiments, with three biological replicates each (n=6).
(C, D) Representative autoradiogram and immunoblots of protein extracts from *Atf4*$^{+/+}$ and *Atf4*$^{-/-}$ MEFs grown in the presence of serum and treated with vehicle (Veh) or rapamycin (20 nM, Rap, 16 h) and pulse labeled with [^{35}S]-methionine for the final 20 min, with biological duplicates from a representative experiment shown (C) and autoradiograms quantified and graphed as mean ± SEM from two independent experiments, each with 2 biological replicates (n=4) (D).
*p < 0.05, **p < 0.01, ***p < .0001, ns = not significant, calculated for (B, D) via one-way ANOVA with Holm-Sidak method for multiple comparisons.

Figure 6—figure supplement 5

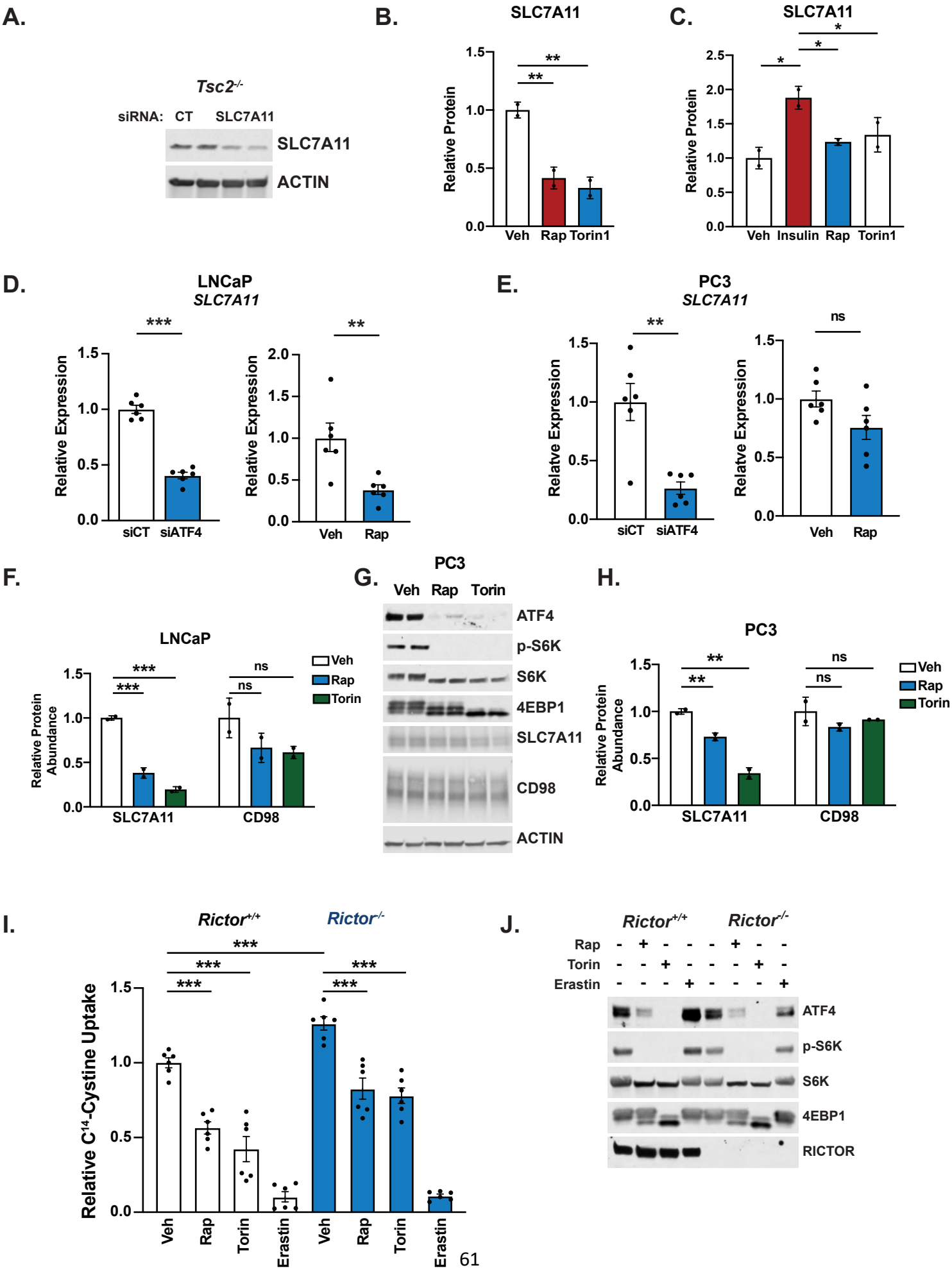

1383 **Supplemental Figure 5. Data related to Figure 6.**
1384 (A) Representative immunoblot of *Tsc2*$^{-/-}$ MEFs transfected with *Slc7a11* or non-targeting
1385 control (siCT) siRNAs prior to serum starvation for 16h.
1386 (B,C) Quantification of representative immunoblots from Figure 6D,E.
1387 (D,E) qPCR analysis of *SLC7A11* transcripts in serum-deprived LNCaP (D) or PC3 (E)
1388 cells either transfected with siRNAs targeting *ATF4* or non-targeting controls (siCT) (left)
1389 or treated with vehicle or rapamycin (20 nM, 16 h) (right). Expression relative to siCT or
1390 vehicle-treated cells is graphed as mean ± SEM from two independent experiments, each
1391 with 3 biological replicates (n=6).
1392 (F) Quantification of representative immunoblots shown in Figure 6F.
1393 (G,H) Representative immunoblot of serum-deprived PC3 cells treated (16 h) with vehicle,
1394 rapamycin (20 nM), or Torin1 (250 nM), shown with biological duplicates (G) and
1395 quantified in (H).
1396 (I,J) Cystine uptake in *Rictor*$^{+/+}$ and *Rictor*$^{-/-}$ MEFs in grown in full serum and treated with
1397 vehicle, rapamycin (20 nM, 24 h), Torin1 (250 nM, 24h), or erastin (10μM, 30') was
1398 assayed and graphed as in Figure 6J relative to vehicle-treated *Rictor*$^{+/+}$ cells with data
1399 from two independent experiments, with three biological replicates each (n=6).
1400 Representative immunoblots shown in (J).
1401 (A,G,J) are representative of two independent experiments.*$p < 0.05$, **$p < 0.01$, ***$p <$
1402 0.001, ns = not significant, calculated for (D,E) via unpaired two tailed t-test and (B,C,F,H,
1403 I) via one-way ANOVA with Holm-Sidak method for multiple comparisons.

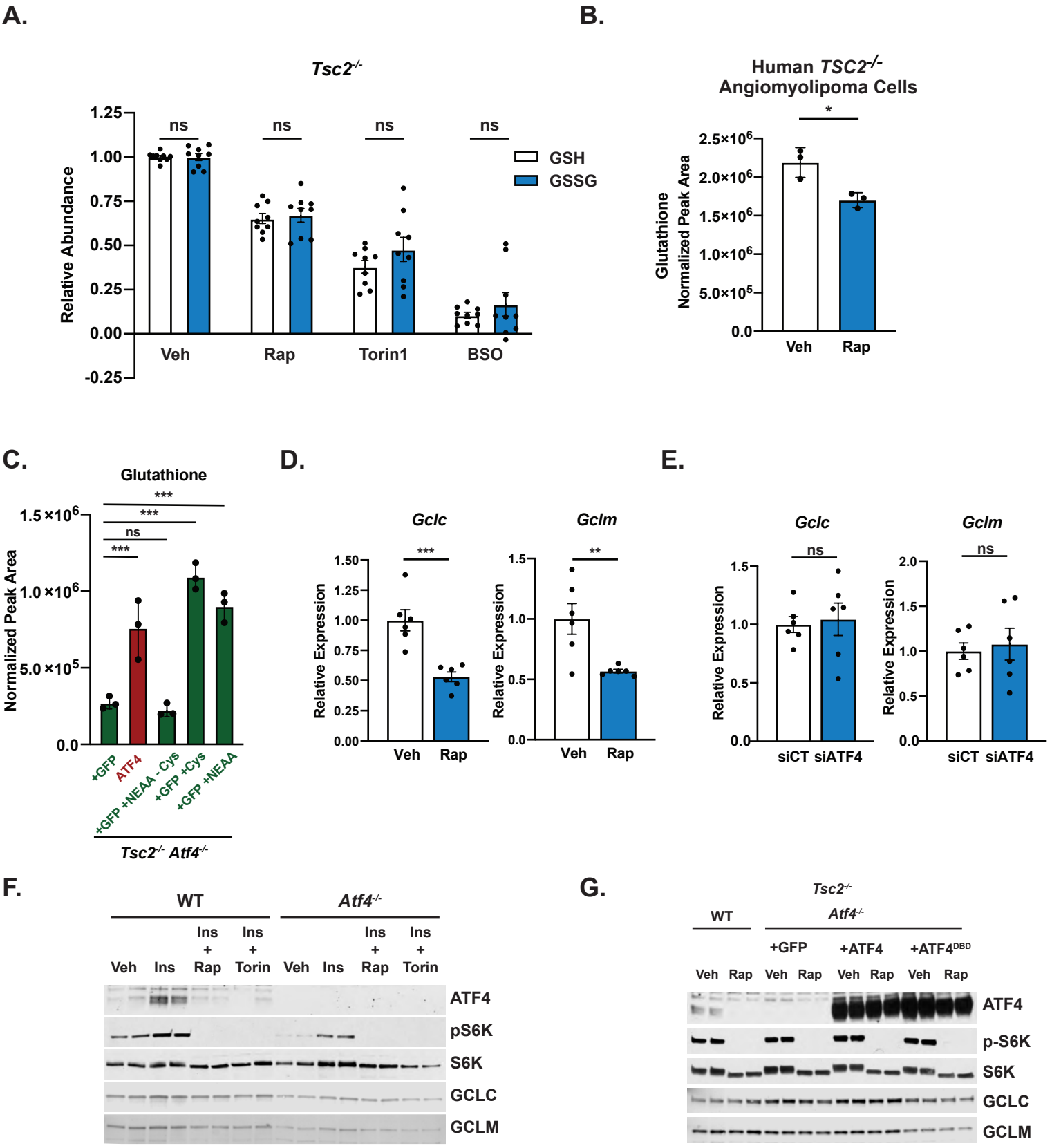

Supplemental Figure 6. Data related to Figure 7.
(A) Relative GSH and GSSG levels in serum-deprived *Tsc2*$^{-/-}$ MEFs treated with rapamycin (20 nM,16 h), Torin1 (250 nM, 16 h), or BSO (10 μM, 16 h). GSH and GSSG levels relative to vehicle-treated cells are graphed as mean ± SEM from three independent experiments, with 3 biological replicates each (n=9).

1409 (B) Total glutathione levels in human *TSC2*$^{-/-}$ angiomyolipoma cells treated with vehicle
1410 or rapamycin (20 nM, 24 h) measured by LC-MS/MS (mean ± SD, n=3).
1411 (C) Normalized peak area of reduced glutathione from LC-MS/MS analysis of serum-
1412 deprived *Tsc2*$^{-/-}$ *Atf4*$^{-/-}$ MEFs with addback of GFP or ATF4 in the presence of
1413 supplemented cysteine (1 mM), non-essential amino acids without cysteine (100 μM
1414 each), or nonessential amino acids (1 mM cysteine or 100 μM) (mean ± SD, n=3).
1415 (D,E) Transcript abundance of *Gclc* and *Gclm* in serum-deprived *Tsc2*$^{-/-}$ MEFs treated
1416 with vehicle or rapamycin (20 nM, 16 h) (D) or transfected with siRNAs targeting *Atf4* or
1417 non-targeting controls (siCT) (E). Expression relative to vehicle (D) or siCT(E) is graphed
1418 as mean ± SEM from two independent experiments, each with 3 biological replicates
1419 (n=6).
1420 (F, G) Representative immunoblots of cells treated as in Figures 7G,H, accept where
1421 indicated in (F), cells were treated with Torin1 (250 nM), with biological duplicates
1422 provided for each condition.
1423 (C, F,G) are representative of two independent experiments. *$p < 0.05$, **$p < 0.01$, ***$p <$
1424 0.001, ns = not significant calculated for (A,C) via one-way ANOVA with Holm-Sidak
1425 method for multiple comparisons and unpaired two tailed t-test for (B,D,E).